70

MARTIN MARIETTA ENERGY SYSTEMS LIBRARIES
3 4456 0361218 8

CENTRAL RESEARCH LIBRARY
DOCUMENT COLLECTION

ORNL-2603
Physics and Mathematics

Cy. 70

AN INVESTIGATION OF THERMAL-TRANSIENT DECAY AT A FLUID-SOLID INTERFACE AND IN TURBULENT FLOW THROUGH CIRCULAR DUCTS

J. J. Keyes, Jr.
J. E. Mott

CENTRAL RESEARCH LIBRARY
DOCUMENT COLLECTION
LIBRARY LOAN COPY
DO NOT TRANSFER TO ANOTHER PERSON
If you wish someone else to see this document, send in name with document and the library will arrange a loan.

OAK RIDGE NATIONAL LABORATORY
operated by
UNION CARBIDE CORPORATION
for the
U.S. ATOMIC ENERGY COMMISSION

LEGAL NOTICE

This report was prepared as an account of Government sponsored work. Neither the United States, nor the Commission, nor any person acting on behalf of the Commission:

A. Makes any warranty or representation, express or implied, with respect to the accuracy, completeness, or usefulness of the information contained in this report, or that the use of any information, apparatus, method, or process disclosed in this report may not infringe privately owned rights; or

B. Assumes any liabilities with respect to the use of, or for damages resulting from the use of any information, apparatus, method, or process disclosed in this report.

As used in the above, "person acting on behalf of the Commission" includes any employee or contractor of the Commission to the extent that such employee or contractor prepares, handles or distributes, or provides access to, any information pursuant to his employment or contract with the Commission.

ORNL-2603

Contract No. W-7405-eng-26

Reactor Projects Division

AN INVESTIGATION OF THERMAL-TRANSIENT DECAY AT A FLUID-SOLID INTERFACE AND IN TURBULENT FLOW THROUGH CIRCULAR DUCTS

J. J. Keyes, Jr.
J. E. Mott

DATE ISSUED

DEC 2 1958

OAK RIDGE NATIONAL LABORATORY
Oak Ridge, Tennessee
Operated by
UNION CARBIDE CORPORATION
for the
U. S. ATOMIC ENERGY COMMISSION

MARTIN MARIETTA ENERGY SYSTEMS LIBRARIES
3 4456 0361218 8

TABLE OF CONTENTS

	Page
ABSTRACT	1
NOMENCLATURE	2
INTRODUCTION	4
ANALYSIS	7
Case I: Local Radial Attenuation at an Interface	7
Case II: Axial Attenuation in Circular Ducts	13
APPARATUS AND EXPERIMENTAL TECHNIQUES	19
OPERATION	25
EXPERIMENTAL RESULTS AND DISCUSSION	28
Case I: Local Radial Attenuation at a Fluid-Solid Interface	28
Case II: Axial Decay in Circular Ducts	33
DISCUSSION OF EXPERIMENTAL ERRORS	44
CONCLUSIONS	46
ACKNOWLEDGEMENT	46
REFERENCES	47
APPENDIX I	48
APPENDIX II	51

LIST OF FIGURES

Fig. No.		Page
1	Dimensionless η Plot for Case of Adiabatic Wall of Thickness ℓ with Surface Coefficient h and Sinusodial Fluid Temperature (Equation 13)	11
2	Frequency Dependence of η Ratio for Finite Adiabatic and Infinitely Thick Plates	12
3	Plot of cos ϵ Correction for Finite and Infinite Plates	16
4	Decay of Sinusoidal Fluid Temperature Oscillations in an Inconel Pipe	18
5	Temperature Oscillation	20
6	Flow Diagram of High Frequency Thermal Cycling Water Test	22
7	Detail of "Gunbarrel" Thermocouple Installation	24
8	Ratio of Wall Temperature Amplitude to Fluid Temperature Amplitude, η, as a Function of Frequency, f, for a Thick-Walled Inconel Tube with a Water Film Heat-Transfer Coefficient of 2675 Btu/hr·ft^2·°F	29
9	Ratio of Wall Temperature Amplitude to Fluid Temperature Amplitude, η, as a Function of Frequency, f, for a Thick-Walled Inconel Tube with a Water Film Heat-Transfer Coefficient of 3700 Btu/hr·ft^2·°F	30
10	Ratio of Wall Temperature Amplitude to Fluid Temperature Amplitude, η, as a Function of Frequency, f, for a Thick-Walled Inconel Tube with a Water Film Heat-Transfer Coefficient of 5000 Btu/hr·ft^2·°F	31
11	Axial Attenuation in a Plastic Tube Illustrating Velocity Profile Mixing	34
12	Axial Attenuation in a Plastic Tube Illustrating Velocity Profile Mixing	35
13	Variation of Axial Attenuation with Flow Rate, Cross-Plot from Figures 11 and 12	36
14	Comparison of Velocity Profile Mixing with Theory: Flow and Frequency Dependence	38

LIST OF FIGURES (continued)

Fig. No.		Page
15	Axial Attenuation in an Inconel Pipe: Comparison of Experiment with Theory	39
16	Axial Attenuation in an Insulated Thin-Wall Inconel Tube: Comparison of Experiment with Theory	41
17	Axial Attenuation in an Insulated Thin-Wall Inconel Tube: Comparison of Experiment with Theory	42
18	Axial Attenuation in a Thin-Wall Insulated Tube: Flow and Frequency Dependence	43

AN INVESTIGATION OF THERMAL-TRANSIENT DECAY AT A FLUID-SOLID INTERFACE AND IN TURBULENT FLOW THROUGH CIRCULAR DUCTS

J. J. Keyes, Jr. J. E. Mott

ABSTRACT

Analytical and experimental heat-transfer studies are presented which are related to attenuation of relatively high-frequency thermal oscillations in fluid-solid systems. Oscillations in fluid temperature may originate in certain high-flux reactors and can cause thermal fatigue failure of metal components. It is of interest to know to what extent these oscillations will be felt at a metal surface and how they might decay in passage through reactor flow channels. Thus, the studies reported herein are intended to aid in the analysis of cyclic thermal stress effects.

The cases studied include:

a) Local radial attenuation of sinusoidal fluid temperature oscillations at the surface of a thick-walled plate or pipe.

b) Axial decay of sinusoidal fluid temperature oscillations in circular ducts for cases of negligible and of appreciable heat exchange with the duct wall.

Agreement of the experimental results with theory is sufficiently accurate for most engineering purposes. Some significant discrepancies are noted, however.

NOMENCLATURE

Letters

A	amplitude, °F
a	radius, ft
b	h/k_w, ft^{-1}
C	a constant multiplier in equation 22
c	heat capacity, Btu/lb-°F
c	constant of integration
G	mass velocity, $lb/hr\text{-}ft^2$
h	film coefficient of heat transfer, $Btu/hr\text{-}ft^2\text{-}°F$
i	$\sqrt{-1}$
j	exponent in equation 22
K	effective axial diffusivity, ft^2/hr
k	thermal conductivity, Btu/hr-ft-°F
L	duct length, ft
ℓ	wall thickness, ft
m	$\sqrt{\frac{\omega}{2\alpha}}$
n	exponent in equation 22
q	heat flux, $Btu/hr\text{-}ft^2$
t	temperature, °F
U	mean velocity, ft/hr
x	distance from surface, ft
Z	axial position, ft

Letters (Continued)

α	thermal diffusivity, ft^2/hr
ϵ	phase angle, radians
θ	temperature excess, $t(x,\tau) - t_{em}$, °F
τ	time, hr
Φ	phase angle, radians
ω	angular frequency, hr^{-1}

Subscripts

e	environment
i	interface
m	mean
w	wall

Dimensionless Terms

$\frac{A(L)}{A(0)}$	total axial attenuation ratio
$\left[\frac{A(L)}{A(0)}\right]^*$	total axial attenuation ratio corrected for wall heat transfer
f	Fanning friction factor
η	surface thermal attenuation ratio, A_i/A_e

INTRODUCTION

Generation of thermal instabilities in nuclear reactors can occur by virture of many mechanisms. It is convenient to classify these according to whether the transients arising therefrom are relatively low or relatively high in frequency.

Low frequency transients, say from one cycle per hour to a cycle per minute or so, can arise during reactor start-up or shutdown and in response to load changes, temperature variations, etc. The total number of such cycles during the lifetime of most reactors is usually low, say less than 10^4, and in general they do not cause difficulty from the standpoint of fatigue failure, although stress cracking can occur.

This report is concerned with high frequency transients in the range from a few cycles per minute to many cycles per second. Such transients are inherent in certain types of reactors (to be discussed); and since these transients are generated essentially continuously during the operation of the reactor, they can produce a sufficient number of cycles to cause fatigue cracking even when the thermal amplitude is low.

High frequency transients may originate at the fuel element-coolant interface, or in the fuel itself when the reactor is of the circulating-fuel type. In the former case, turbulent eddies in the coolant medium, which are known to penetrate the thermal boundary layer even in straight pipes with fully developed turbulence,[1] cause rapid fluctuations in the rate of heat removal from the element resulting in surface temperature transients. The magnitude of these transients is dependent on (a) geometrical factors such as entrance conditions, shape and size of flow

passages, etc., (b) the fuel element and coolant thermal properties, (c) the flow characteristics such as Reynolds modulus, (d) the heat-transfer coefficient on the coolant side, and (e) the temperature differential. Boiling heat transfer is particularly likely to cause surface thermal instabilities.

In the case of circulating-fuel reactors in which the fuel-coolant is heated volumetrically in the reactor core, the transient structure of turbulent flow, hydrodynamic instabilities, and adverse temperature profiles can induce severe thermal oscillations in the fluid which will be felt at the core wall and which will persist in the fluid leaving the reactor. Thus, it is of importance to know (a) to what degree metal surfaces will respond to rapid fluctuations in the temperature of the fluid environment and (b) to what extent fluid thermal transients are damped in passage through reactor channels. It is the purpose of this report to present some experimental results obtained in a study of thermal transients related to problems of operation of circulating-fuel reactors in particular, but applicable to other transient cases as well. Special emphasis is placed on understanding the basic mechanisms involved and comparing the experimental results with theory. This work is part of a longer range program which includes, in addition to the low-temperature exploratory research described here, a substantial amount of high-temperature testing of materials subject to high-frequency thermal-cycling conditions and some high-temperature research measurements. It is anticipated that a report will be issued at a later date covering the high-temperature phase of the program.

The first section of this report contains the analytical treatment in which the following cases are considered:

Case I. Local Radial Attenuation of Sinusoidal Temperature Oscillations at a Fluid-Solid Interface

A. Effectively infinite plate, adiabatic

B. Finite plate, adiabatic

C. Finite plate, heat sink (bath) at free face

Case II. Axial Attenuation of Sinusoidal Fluid Temperature Oscillations in Circular Ducts

A. No heat transfer to wall -- "velocity profile mixing"

B. Heat transfer to wall

1. Neglecting "velocity profile mixing"

2. Including "velocity profile mixing"

Data are presented for comparison with Cases I-A and II, utilizing water near room temperature. This work is a continuation of that reported by Mott[2] in which data for Case I-A only were reported.

ANALYSIS

Case I: Local Radial Attenuation at an Interface

Consider fluid flow along a plane thermally conducting surface with the fluid environment temperature, t_e, varying sinusoidally with amplitude A_e about a mean value, $t_{e,m}$:

$$t_e(\tau) = t_{e,m} + A_e \cos \omega\tau \tag{1}$$

Because of thermal inertia (finite thermal diffusivity) of the surface, the interfacial temperature amplitude, A_i, will be less than A_e and will lag the fluid temperature by a phase angle Φ. Thus,

$$t_i(\tau) = t_m + A_i \cos (\omega\tau - \Phi) \tag{2}$$

It is desired, in the first place, to determine the local attenuation ratio, $\eta = A_i/A_e$, for conditions A, B, and C of Case I given on page 6.

The differential equation which applies to heat flow in the solid wall is:

$$\frac{\partial^2\theta(x, \tau)}{\partial x^2} = \frac{1}{\alpha_w} \frac{\partial\theta(x, \tau)}{\partial\tau} \tag{3}$$

where α_w $(= k_w/c_w \rho_w)$ is the thermal diffusivity of the wall material, x is the distance from the fluid-solid interface, and $\theta(x, \tau)$ is the temperature excess, $t(x, \tau) - t_{e,m}$.

This equation can be solved for the three desired conditions when the following assumptions are made:

(1) Physical properties are independent of temperature.

(2) The film coefficient of heat transfer, h, is constant and defined by the equation

$$h = \frac{q}{\theta'(\tau)} \qquad \text{at } x = 0$$

where $\theta'(\tau) = t_e - t_i$ is the instantaneous temperature differential between fluid and interface. Note that this assumption neglects the thermal capacity of the boundary layer.

A. Effectively Infinite Plate, Adiabatic Wall

For this case, it is assumed that there is no net heat transfer and $t_{e,m} = t_m$.

The boundary conditions are:

$$h\theta'(\tau) = k \frac{\partial\theta(x, \tau)}{\partial x} \qquad \text{at } x = 0 \tag{4}$$

$$\frac{\partial\theta(x, \tau)}{\partial x} = 0 \qquad \text{at } x = \infty \tag{5}$$

Jakob[3] presents the steady-state solution of equations 3, 4, and 5 subject to the environment fluctuation given by equation 1:

$$\theta(x, \tau) = A_e \eta\pi \cos(\omega\tau - mx - \epsilon) \tag{6}$$

With the introduction of the dimensionless parameter,

$$\frac{m}{b} = \frac{k_w}{h} \sqrt{\frac{\omega}{2\alpha_w}} \quad , \tag{7}$$

$$m = \sqrt{\frac{\omega}{2\alpha_w}}$$

the attenuation ratio* is given as,

$$\eta = \left[\frac{1}{1 + 2m/b + 2(m/b)^2} \right]^{1/2} \tag{8}$$

$$\epsilon = \tan^{-1} \frac{1}{1 + b/m} \tag{9}$$

$$\pi = \exp\,(-mx) \tag{10}$$

Note that h is the only quantity involving fluid properties. Equation 8 will hereafter be referred to as the "Jakob equation."

B. <u>Finite Plate, Adiabatic</u> (see Appendix I for derivation)

For this case, boundary equation (4) applies; but equation 5 becomes:

$$\frac{\partial\theta(x,\ \tau)}{\partial x} = 0 \qquad \text{at } x = \ell \tag{11}$$

where ℓ is the wall thickness.

The solution for the surface temperature is:

$$\theta(0,\ \tau) = A_e\ \eta \cos\,(\omega\tau - \epsilon') \tag{12}$$

where

$$\eta = \frac{\cosh 2m\ell + \cos 2m\ell}{\left[\delta^2 + (m\beta/b)^2\right]^{1/2}} \tag{13}$$

$$\epsilon' = \tan^{-1}\,(m\beta/b\delta) \tag{14}$$

$$\delta = m/b\ (\sinh 2m\ell - \sin 2m\ell) + (\cosh 2m\ell + \cos 2m\ell)$$

$$\beta = \sinh 2m\ell + \sin 2m\ell$$

---

*Note that equation 8 can also be obtained from equation 13, as derived in Appendix II, by letting $\ell \to \infty$.

Fig. 1 is a dimensionless plot in the form suggested by Platus and Meghreblian[4] of η vs $m\ell$ with m/b as the parameter for the adiabatic wall case. For given values of m and b (i.e., given material properties, frequency, and heat-transfer coefficient), η first decreases as the wall thickness, ℓ, increases, then increases slightly, and finally for $m\ell$ greater than about 2 approaches the asymptotic value given by the Jakob equation for infinite wall. For Inconel, $m \cong 21$ in.$^{-1}$ at 1 cps (see Note on Cylindrical Geometry); thus, for $\ell > 2/21 \cong 0.100$ in., the wall behaves as effectively infinite.

The frequency dependence of η is illustrated in Fig. 2 for Inconel at room temperature and for the cases of effectively infinite and finite wall geometry. The dashed curve is the Jakob equation for a thick plate and the solid one is a plot of equation 13 for the specific case of $\ell = 0.020$ in. Note that the curves cross but approach each other at high frequency, as the value of $m\ell$ increases from 0.42 at 1 cps.

C. Finite Plate with Heat Sink (Bath) at Free Surface

For this case, the boundary condition at the free face is

$$\theta(\ell, \tau) = 0 \tag{15}$$

The solution is presented by Meghreblian and Platus in reference 4.

Note on Cylindrical Geometry

According to Platus[5] effects of curvature do not become important unless the radius is of the order of the characteristic length, $1/m$. For Inconel, as used in this work, $m \cong 21$ in.$^{-1}$ at 1 cps, and the characteristic length is consequently 0.048 in. Since the smallest cylinder used

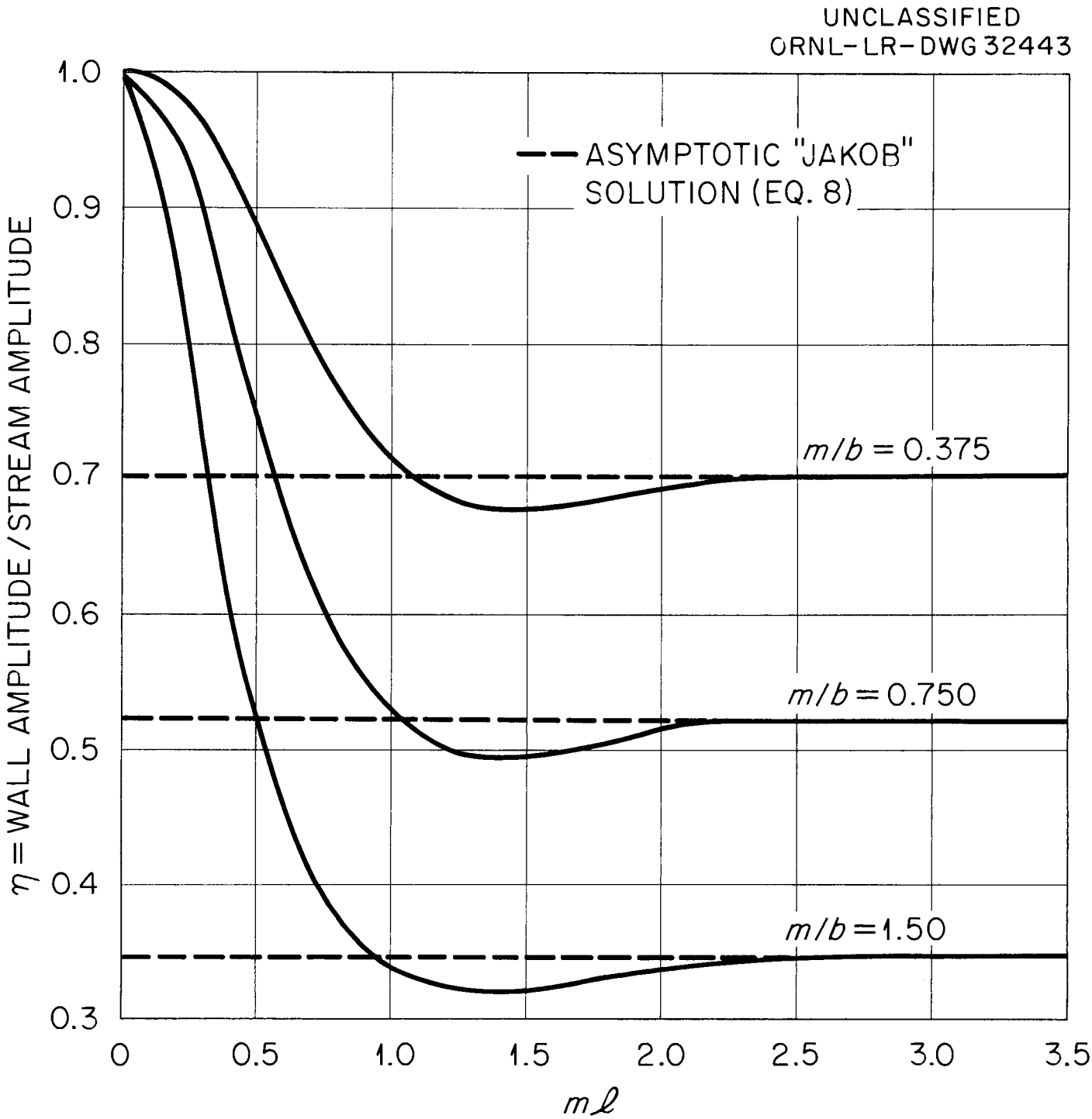

Fig. 1. Dimensionless η Plot for Case of Adiabatic Wall of Thickness ℓ With Surface Coefficient h and Sinusoidal Fluid Temperature (Equation 13).

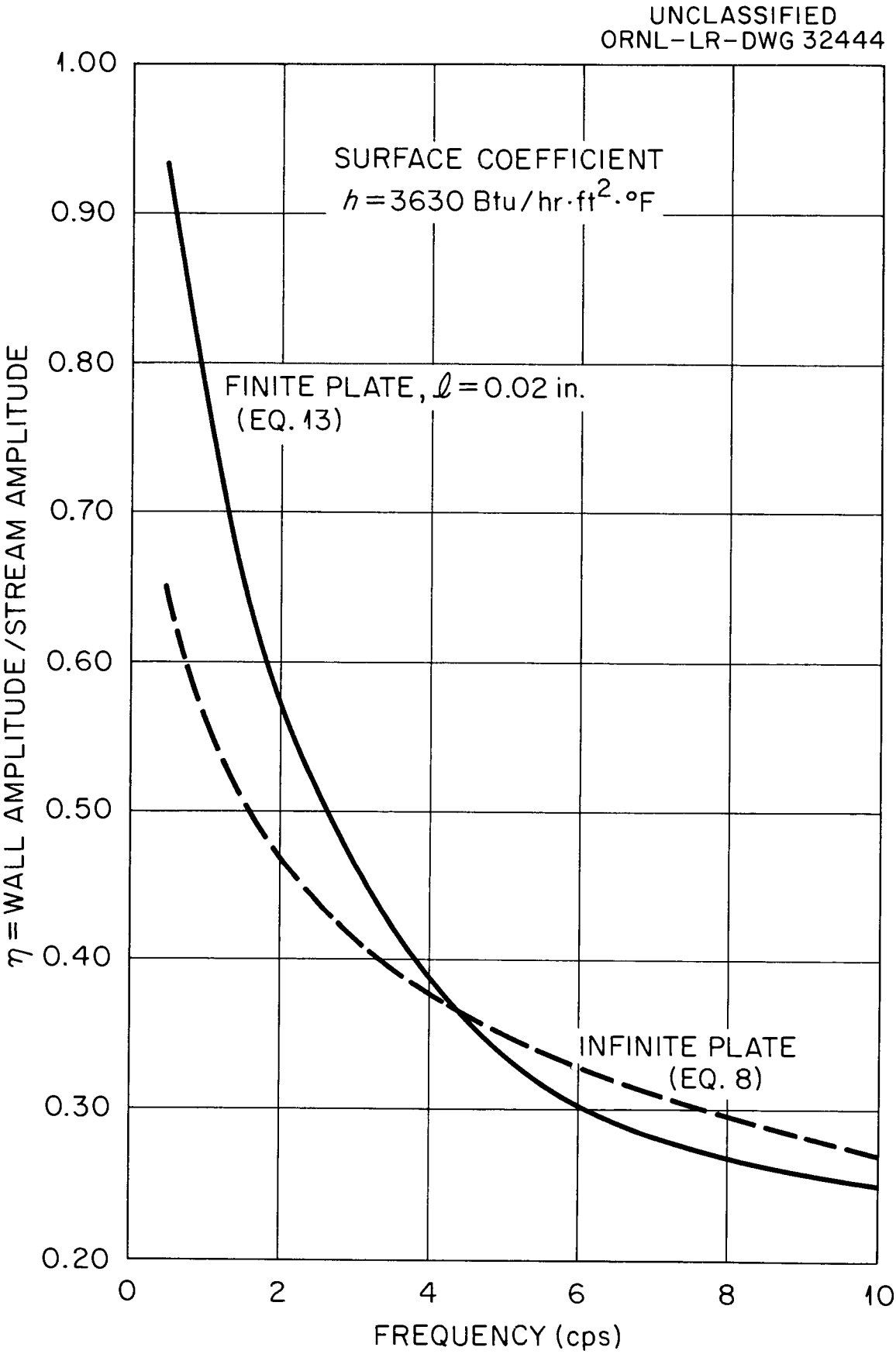

Fig. 2. Frequency Dependence of η Ratio for Finite Adiabatic and Infinitely Thick Plates.

here had a radius of about 5 characteristic lengths, the results derived for plane geometry should be accurate to within a few per cent. Thus no attempt to correct for curvature is made.

Case II: Axial Attenuation in Circular Ducts

Consider flow in a long duct when the inlet fluid temperature is periodic as given by equation 1. If the duct is made of thermally non-conducting material (as approximated by a plastic), two mechanisms can contribute to the observed attenuation of thermal amplitude:

(1) Relative axial motion of fluid elements at different radial positions, arising from the normal velocity profile, cause an instantaneous temperature profile to be established. Turbulent diffusion acting in the radial direction tends to smooth out the profile, and the net result is equivalent to mixing of the wave peaks. This mechanism is referred to herein as "velocity profile mixing."

(2) Turbulent diffusion in the axial direction is a possible contributing factor. However, it will be shown that this is generally negligible in comparison with mechanism (1).

When the wall of the duct is thermally conducting, an additional mechanism becomes important:

(3) Alternate radial heat transfer to and from the wall (corresponding to temperature maxima and minima) causes substantial attenuation of the wave amplitude.

A. Velocity Profile Mixing

The case of turbulent dispersion of matter in a pipe is analyzed by G. I. Taylor[6] who determined an effective coefficient of axial diffusivity, K, to express the interplay of velocity profile and radial diffusion:

$$K = 7.14\ aU\sqrt{f} \tag{16}$$

where a is the internal duct radius; U, the mean velocity; and f, the friction coefficient. Data are presented in which brine was injected into a straight pipe and the conductivity recorded at a point downstream. These data verify equation 16. Tichacek et al.[7] have applied a modification of Taylor's analysis to mixing in liquid and gas flow in straight pipes.

In order to apply this definition of an effective axial diffusivity to the case of interest, it is necessary to regard the process of radial thermal transport under the influence of a velocity profile as analogous to one of axial diffusion in which the effective axial diffusivity defined by Taylor is applicable. Keyes[8] has derived an expression for the axial attenuation of a sinusoidal fluid composition or temperature oscillation due to longitudinal eddy diffusivity, K:

$$\frac{A(L)}{A(0)} = \exp\left(-\frac{\omega^2 LK}{U^3}\right) \tag{17}$$

where A(L) is the fluid thermal amplitude at a distance L downstream from a position where the amplitude is A(0).

Combining equations 16 and 17:

$$\frac{A(L)}{A(0)} = \exp\left\{-\frac{7.14\ \omega^2 Laf^{1/2}}{U^2}\right\} \tag{18}$$

J. J. Thompson[9] treats the same problem but in more detail to include the case of liquid metals. His result, corresponding to equation 18, is:

$$\frac{A(L)}{A(0)} = \exp\left\{ - \frac{UL}{2K}\left[\left(1 + \frac{1}{2}\left\{ \left\{ 1 + \frac{16\,\omega^2K^2}{U^4} \right\}^{1/2} - 1 \right\} \right)^{1/2} - 1 \right]\right\} \tag{19}$$

Note, however, that in most practical cases for highly turbulent flow and frequencies less than 10 to 20 cps, $(16\,\omega^2K^2/U^4) << 1$. Equation 19 then reduces to equation 17 identically.

B. Heat Transfer to Wall

As has been indicated (page 13) when the wall can absorb heat from the fluid, an additional mechanism for axial damping exists. It will be assumed that this mechanism is independent of velocity profile mixing, so that the resulting solutions can be combined linearly to give the over-all result.

1. Considering wall heat transfer alone, an approximate relationship between the stream amplitude attenuation ratio, $A(L)/A(0)$, of a sinusoidal fluid temperature wave in a round duct and the local attenuation ratio, η, between fluid and duct wall is derived in Appendix II:

$$\frac{A(L)}{A(0)} \cong \exp\left[- \frac{2hL\,(1 - \eta \cos \epsilon)}{a\rho c U} \right] \tag{20}$$

where η and ϵ are given by the appropriate equations 8, 9, 13, and 14. Fig. 3 is a plot from which $\eta \cos \epsilon$ can be determined for two cases of interest.

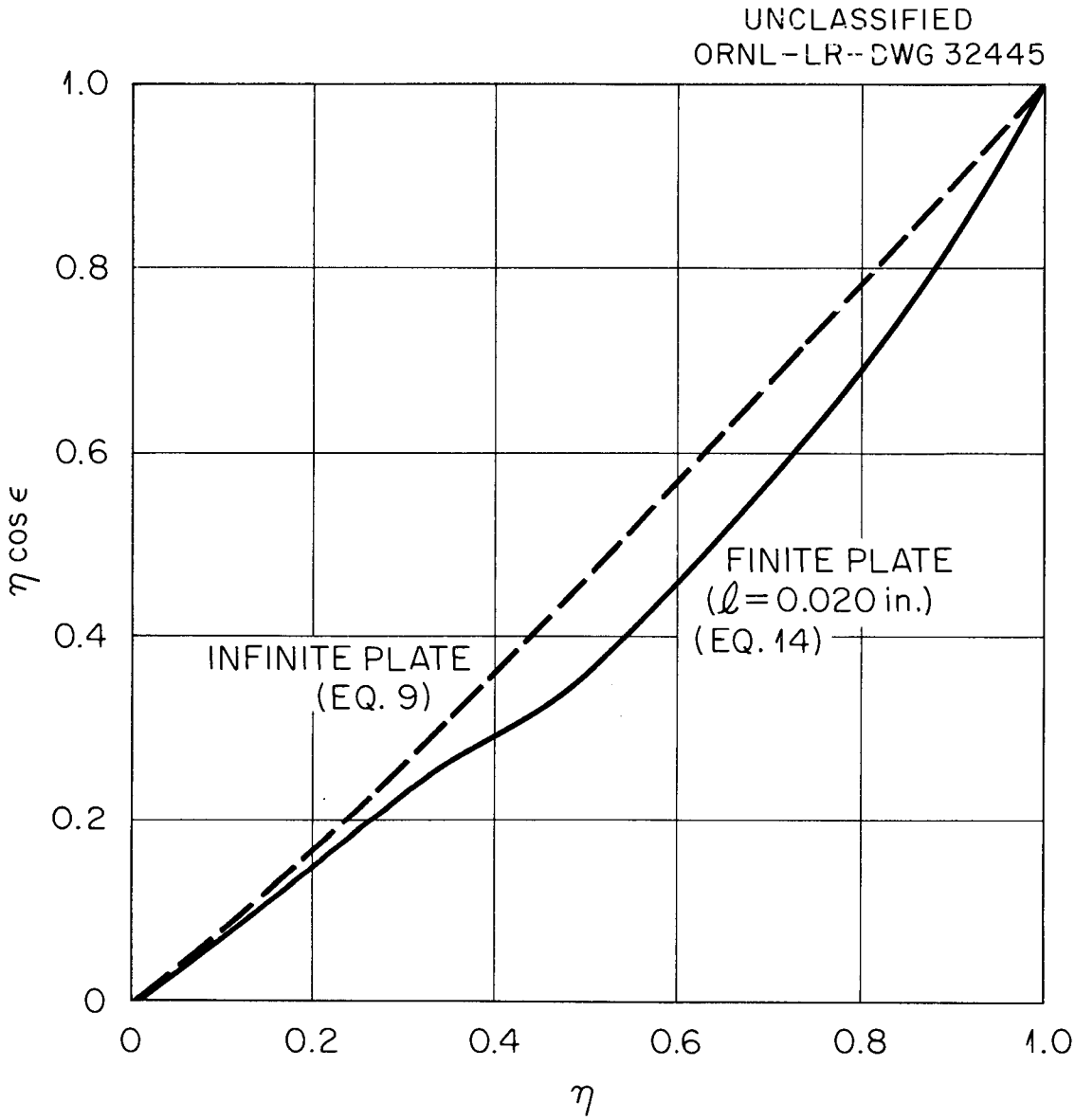

Fig. 3. Plot of cos ϵ Correction for Finite and Infinite Plates.

2. When the damping attributable to velocity profile mixing (equation 18) is combined linearly with that given by equation 20, the final result for axial attenuation in circular ducts with thermally conducting walls is:

$$\frac{A(L)}{A(0)} \cong \exp\left\{ - \frac{L}{a}\left[\frac{2h\,(1 - \eta \cos \epsilon)}{\rho c U} + \frac{7.14\,\omega^2\, a^2\, f^{1/2}}{U^2} \right]\right\} \qquad (21)$$

Observe that when the frequency is low, the second term on the right (inside the braces) becomes negligibly small and essentially all of the damping arises from wall heat transfer; whereas, as the frequency is increased, a substantial fraction of the over-all attenuation arises as a consequence of velocity profile mixing. This is illustrated in Fig. 4 in which equations 18, 20, and 21 are plotted separately. A simplified approximate form of equation 21 is given later.

Note that $\ln \frac{A(L)}{A(0)}$ is linear in duct length, L. Also, it can be shown by substitution in equation 21 that the longitudinal decay increases rapidly with radius, a, for a given mass flow, so that large pipes are more effective in damping thermal oscillations than are small ones.

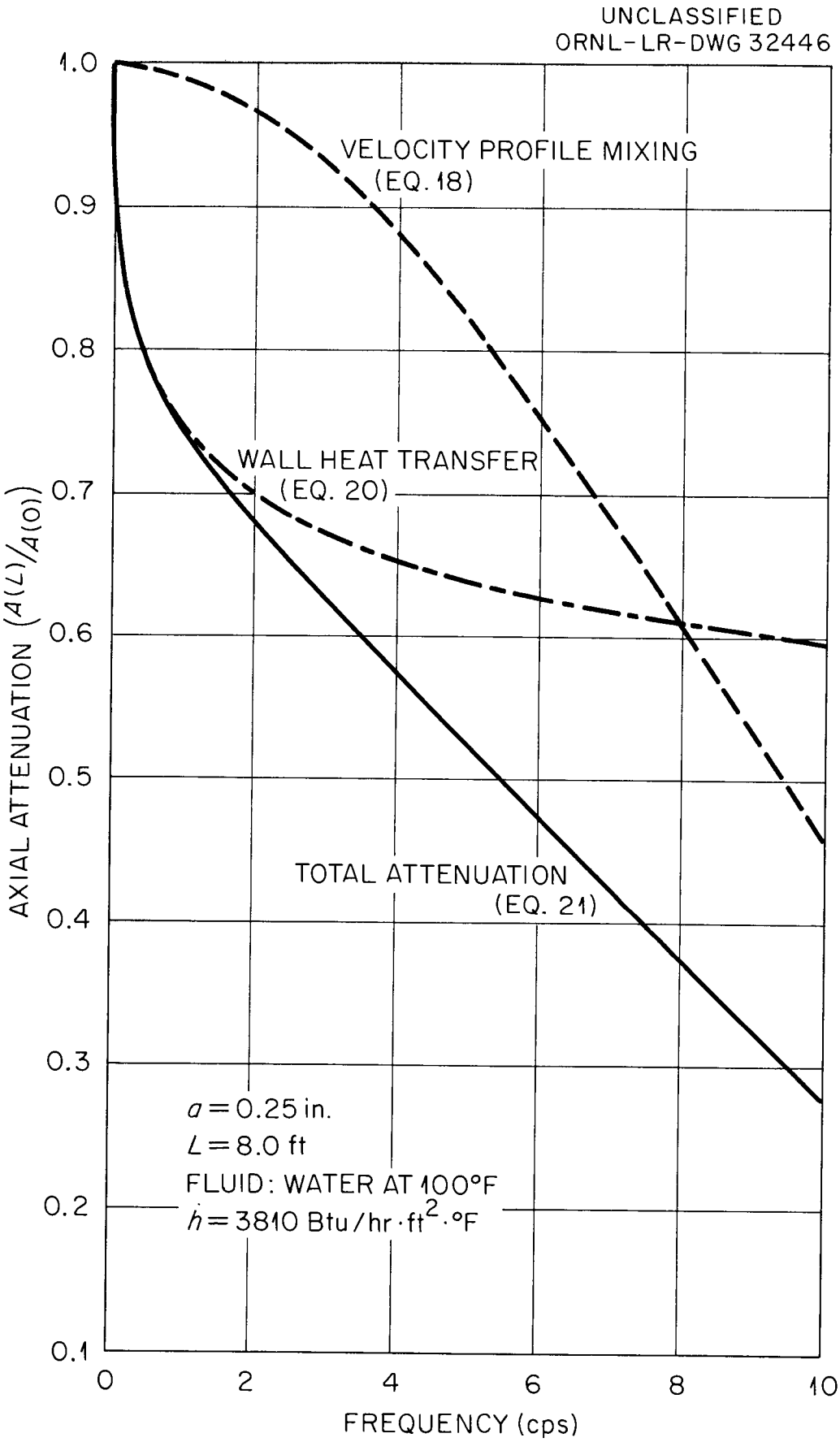

Fig. 4. Decay of Sinusoidal Fluid Temperature Oscillations in an Inconel Pipe.

APPARATUS AND EXPERIMENTAL TECHNIQUES

Two problems had to be solved in order that a meaningful experimental evaluation of the theoretically predicted surface attenuation and longitudinal decay ratios could be undertaken. First, suitable equipment for generating sinusoidal fluid temperature oscillations at frequencies up to 10 cps had to be developed so that the boundary condition (equation 1) could be adequately simulated. Second, thermocouple techniques had to be developed for measurement of transient temperatures in the fluid stream and at precisely the inside pipe wall with negligible attenuation and without disturbing the interfacial fluid heat transfer or wall thermal continuity. These two problems will be considered separately.

Fig. 5 is a schematic diagram of the pulse pump used for generation of sinusoidal fluid temperature oscillations in the mixed fluid discharge line. Two bellows-sealed, reciprocating pistons (4-in. diameter x 1/2-in. stroke) driven in phase opposition by means of a scotch-yoke harmonic drive mechanism, are employed to provide pulsating gas pressure to a pair of pulse chambers holding the working fluid, in this case water at two different temperatures. Thus, alternate slugs of hot and cold fluid are injected into the common line leaving the "Y". Operation is such that one pulse chamber is filling while the other is emptying (note arrows), thus preserving constant flow to the test section. Fig. 5-B illustrates the relationship of the oscillating thermal output to the available hot and cold fluid temperatures. The efficiency of the pulse pump is such as to deliver up to 25% of the available Δt to the mixed fluid stream at 10 cps, and a total flow rate of 16 gpm, with proportionally higher efficiency at lower frequencies

UNCLASSIFIED
ORNL-LR-DWG 32447

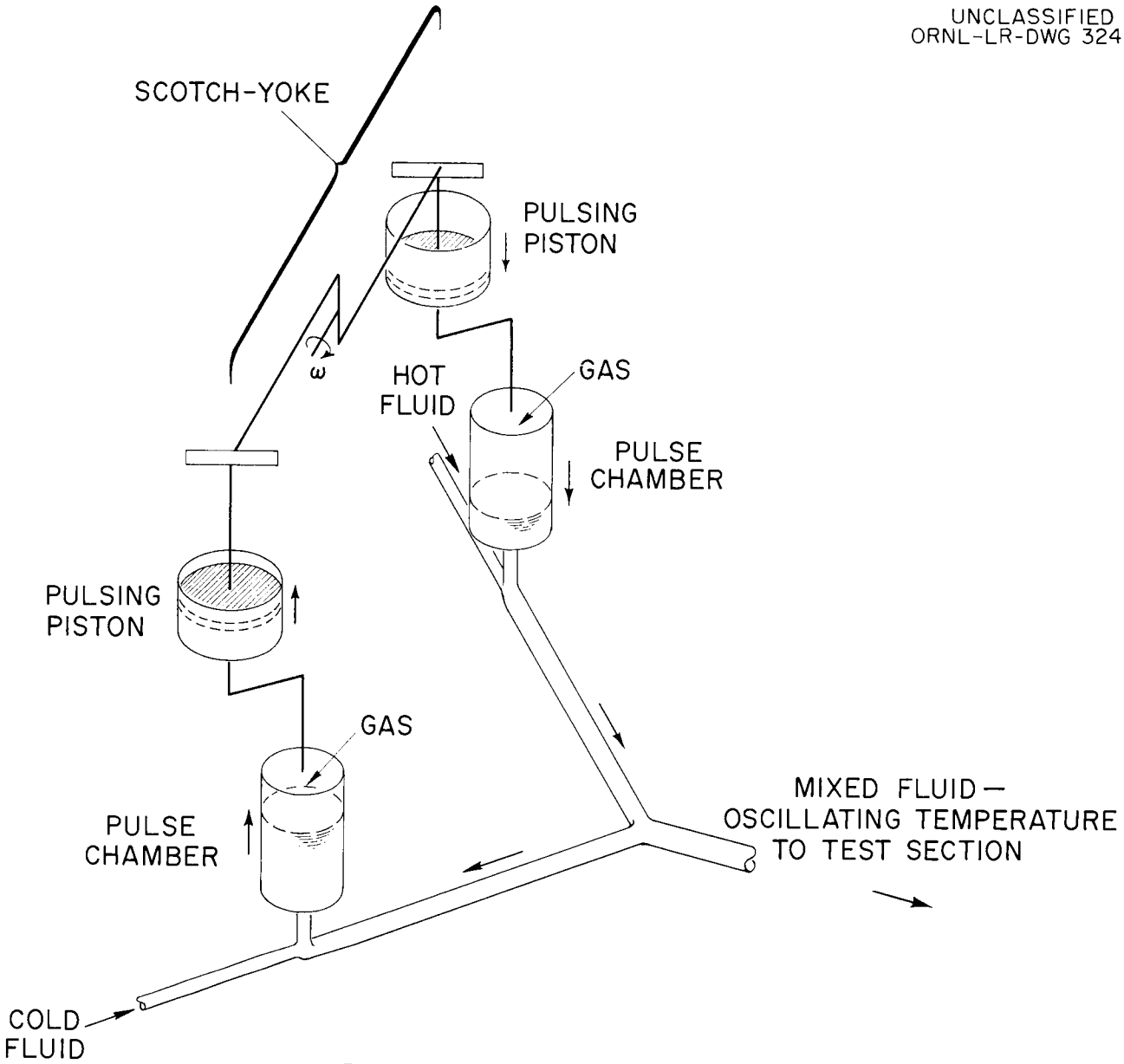

PULSE-PUMP SCHEMATIC

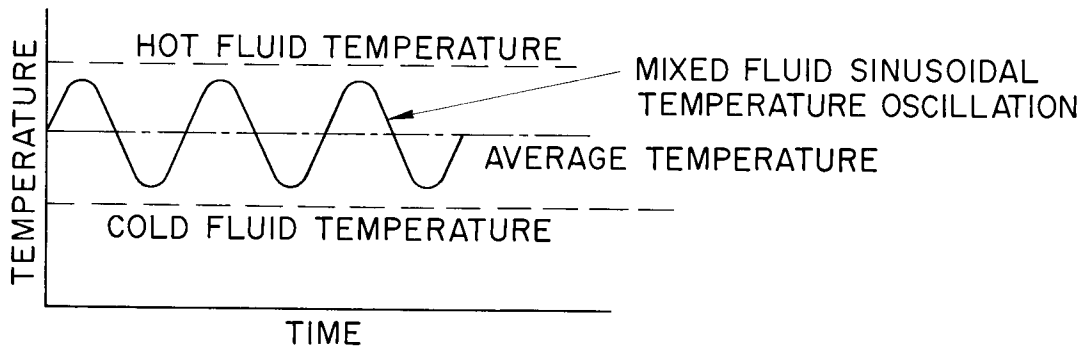

TEMPERATURE OSCILLATION

Fig. 5

and/or flow rates.* An analysis of pulse pump performance with liquids of different densities will be presented in a future report.

Fig. 6 is a flow diagram of the apparatus. Note that a baffled 50-gal hold-up tank was used to deaerate the hot water supply. Flow rates of hot and cold water were read with calibrated rotameters.

Two types of test section were employed, according to whether the local surface attenuation, η, or longitudinal decay, $A(L)/A(0)$, was to be measured. For the former, the section was a 0.470-in. ID x 0.250-in. wall Inconel pipe with an entrance length ahead of the position of a measurement of 24 in. ($x/d \cong 50$). Instantaneous fluid temperatures were measured with a 36-gauge (0.005-in. OD) Inconel-nickel wire thermocouple (formed by a butt-welding technique to minimize junction size) positioned with the junction at mid-stream** and slightly downstream from the surface thermocouple described below. The stream thermocouple was found experimentally to have a time constant of less than 3.5 milliseconds and to attain 95% of a total step temperature change in 15 miliseconds. Thus, frequencies of up to 30 cps could be accurately followed.

Surface temperature variations were measured by a modification of the "gunbarrel" thermocouple technique developed by the Germans during World War II. A thermocouple of this type, manufactured by Midwest Research Company and consisting of a heavy-walled Inconel tube tightly surrounding

---

*Larger piston displacements than employed here would enable attainment of proportionately higher efficiencies, other conditions remaining equal.

**Because of the high level of turbulence, there was no observable effect of thermocouple location within ± 0.20 in. of mid-stream, and it can be assumed that the couple was reading very nearly mixed-mean fluid temperature amplitude.

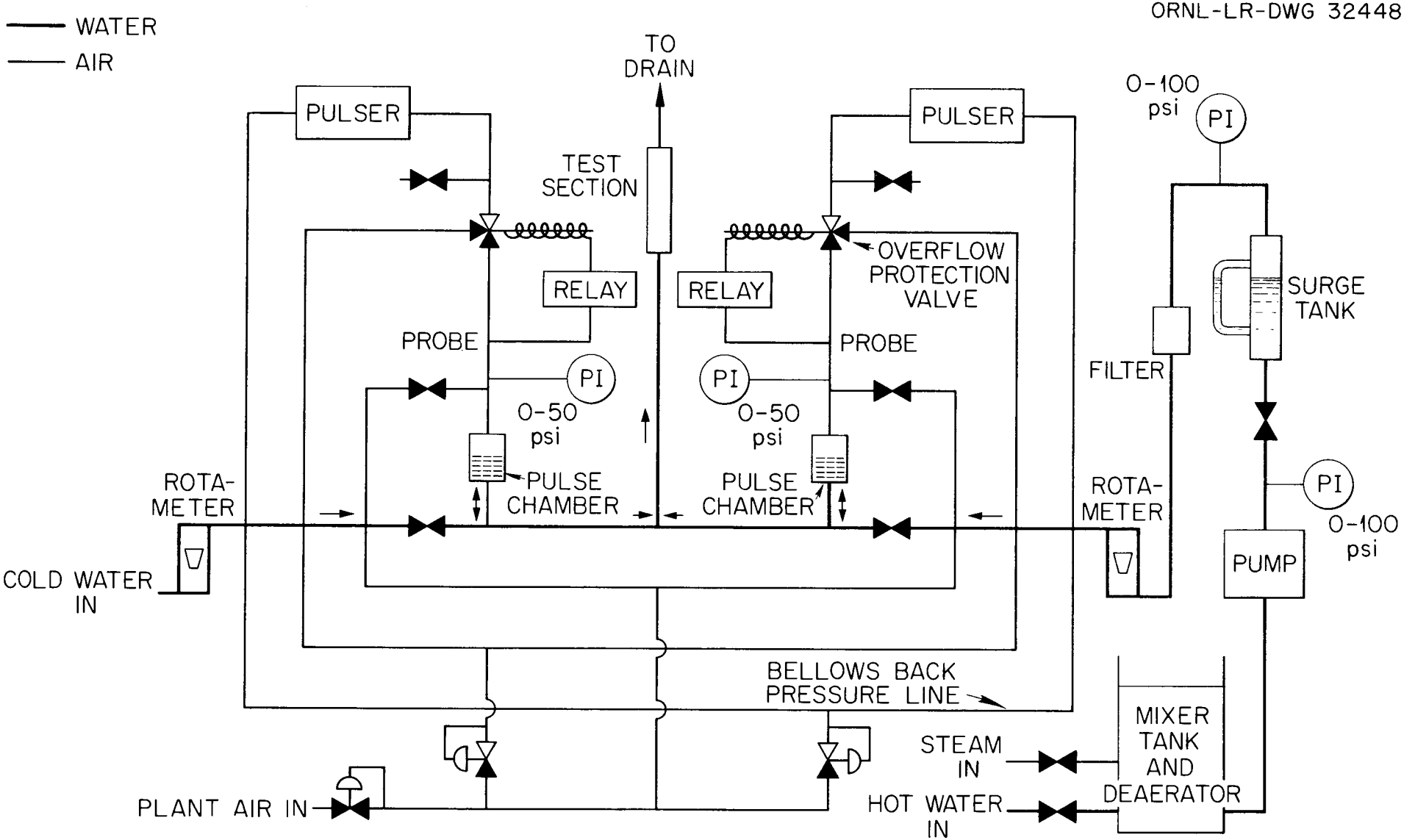

Fig. 6. Flow Diagram of High Frequency Thermal Cycling Water Test.

a small oxidized nickel wire which serves as one lead of the couple, was shrunk fit into the Inconel test-section wall. The section was then reamed such that the end of the thermocouple was made flush with the inside surface. A thin (~ 1 micron) layer of nickel deposited by vacuum evaporation onto the end of the couple formed the active junction. Fig. 7 illustrates the thermocouple construction and installation. Since Inconel comprised 98% of the mass of the couple, it is believed that interruption of thermal continuity of the wall by the nickel wire and coating has negligible effect on the measured temperature amplitude. Furthermore, the response of the couple is practically instantaneous due to the extremely low mass of the coating.

For measuring axial attenuation of fluid temperature amplitude, the test sections consisted of 10-ft lengths of the appropriate pipe or tubing: 3/8-in. Schedule 40 Inconel pipe, 1/2-in. OD x 0.020-in. wall Inconel tubing,* and 5/8-in. OD x 0.065-in. wall polystyrene tubing were employed (see Table II). Thirty-six-gauge chromel-alumel stream thermocouples, similar to the type already described, were positioned 8-ft apart with the junctions mid-stream. An entrance region of about 25 diameters was provided ahead of the first thermocouple.

All temperatures were recorded on a Brush Model 202 Oscillograph, using a Kay-Lab Model III d-c preamplifier and a High-Gain, Model BL-550 d-c Brush amplifier. A Kay-Lab 60 cps filter ahead of the preamplifier was necessary to eliminate stray pick-up. Over-all response of the system was measured to be flat to above 10 cps.

---

*Well insulated with glass wool and aluminum foil.

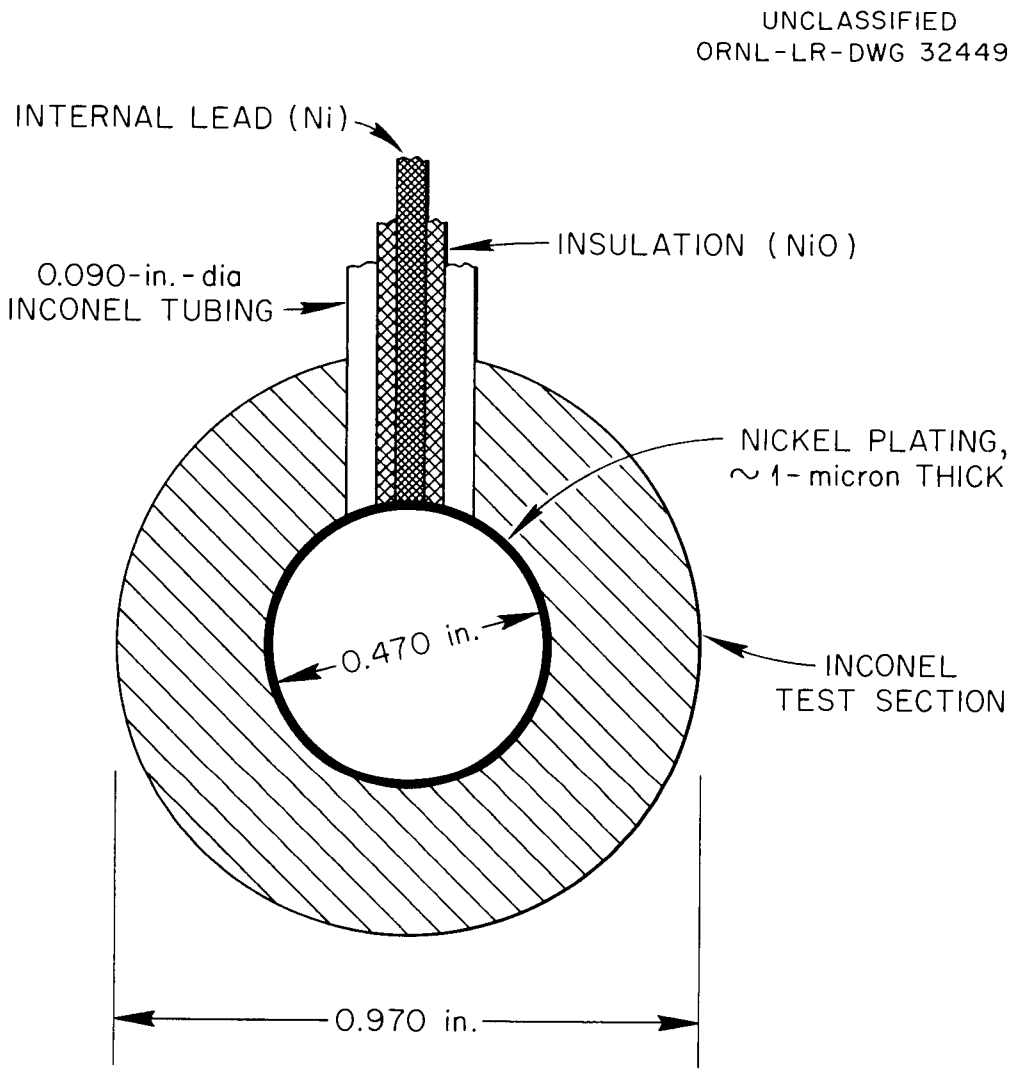

Fig. 7. Detail of "Gunbarrel" Thermocouple Installation.

OPERATION

The surface and mid-stream thermocouples were calibrated before each run at the hot and cold stream temperatures by operating the system isothermally (no pulse) and as nearly adiabatically as possible. Flows and temperatures were then set so that the mean bulk temperature of the mixed hot and cold streams was equal to ambient to reduce net heat exchange with the environment; see Table I for typical operating conditions. With the pulser operating, the fluid temperature amplitude at the test section was at most no greater than ± 15% of the mean fluid temperature. This was controlled by introducing a variable length of 1-in. Schedule 40 pipe ahead of the test section to serve as an attenuator and low-pass filter for harmonic elimination; the wave delivered to the test section was thus very nearly sinusoidal.

The surface attenuation ratio, η, was obtained directly by measuring the amplitude of the wall thermocouple reading and dividing by that of the stream thermocouple, with appropriate calibration factors. Note that errors which might arise in absolute temperature measurement due to spurious junctions, etc., are eliminated here, since only temperature differences are involved. Likewise, for the decay measurements, the ratio $A(L)/A(0)$ of downstream to upstream amplitude is obtained directly. Operating conditions for Cases I-A and II-A, B (page 6) are summarized in Tables I and II.

TABLE I. SUMMARY OF OPERATING CONDITIONS

Case I-A: Local Surface Attenuation Ratio, η, in a Thick-Walled Pipe

Test-Section Geometry	Run a	Run b	Run c
Mixed Flow Rate (gpm)	8.3	12.8	18.0
Mean Reynolds Number	64,000	99,100	143,700
Mean Water Temperature (°F)	80	80	80
Hot Water Temperature (°F)	100	100	100
Cold Water Temperature (°F)	60	60	60
Mean Heat-Transfer Coefficient (Btu/hr-ft^2-°F)	2,675	3,700	5,000

TABLE II. SUMMARY OF OPERATING CONDITIONS

Cases II-A & II-B: Axial Attenuation in Pipes and Tubes

CASE II	A				B					
Test-Section Geometry	5/8-in. OD x 0.065-in. Wall Polystyrene Tube L = 8 ft				3/8-in. Schedule-40 Inconel Pipe L = 8 ft		1/2-in. OD x 0.020-in. Wall Inconel Tube L = 6 ft			
Mixed Flow Rate (gpm)	4	8	12	16	15.2	10	15	12	10	8
Mean Reynolds Number (x 10^{-3})	36	72	107	143	137	90	120	96	80	64
Mean Water Temperature (°F)	100	100	100	100	100	100	80	80	80	80
Mean Heat-Transfer Coefficient (Btu/hr-ft^2-°F)	1585	2755	3810	4780	4470	3200	4580	3832	3310	2769

EXPERIMENTAL RESULTS AND DISCUSSION

Case I. Local Radial Attenuation at a Fluid-Solid Interface

A. Effectively Infinite Wall, Adiabatic

The results for water in an Inconel pipe are shown in Figs. 8, 9, and 10 in which η is plotted as a function of frequency for three values of the film coefficient calculated from the operating conditions listed in Table I using the Dittus-Boelter[10] equation*:

$$N_{Nu} = 0.023\ N_{Re}^{0.8}\ N_{Pr}^{0.35} \tag{23}$$

A comparison is made with the theoretical equation of Jakob (equation 8) for a thick-plate geometry. Table III lists the properties of Inconel used in the calculations. The results indicate that equation 8 applies with reasonable accuracy, the greatest deviations occurring at the lower frequencies where the measured η ratios fall 8 to 12% above theory.

The three sets of duplicate tests in Fig. 10 illustrate the degree of reproducibility attainable. Perhaps the greatest discrepancy between test conditions and the assumptions used in the deviations occurs as a result of variation in h with temperature. By keeping the temperature amplitude as low as possible consistent with the accuracy of measurement, h was never permitted to vary more than ± 5% about the mean.

No surface attenuation measurements corresponding to Cases I-B and C have been made.

---

*The exponent of 0.35 on N_{Pr} was chosen as a compromise for alternate heating and cooling.

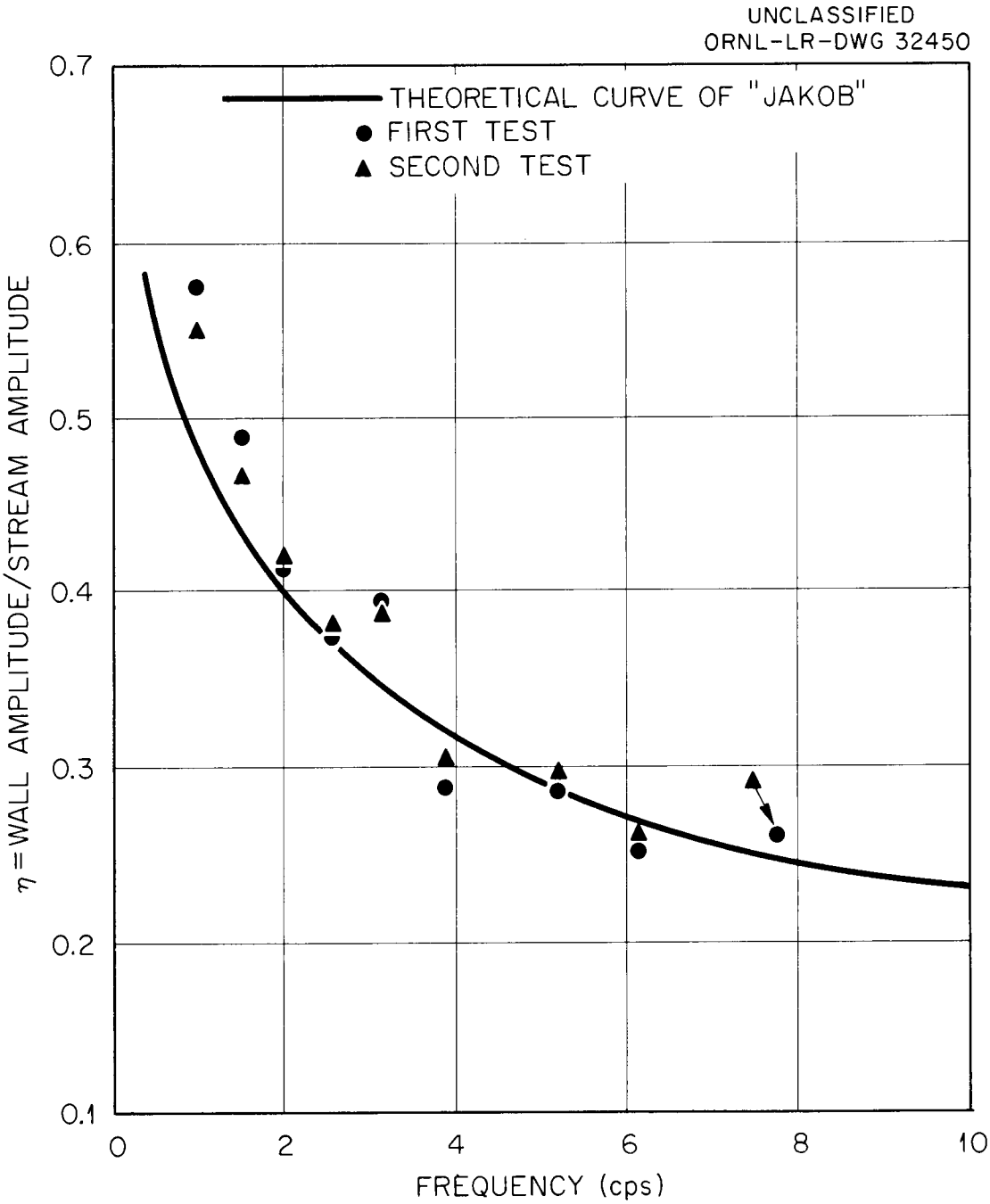

Fig. 8. Ratio of Wall Temperature Amplitude to Fluid Temperature Amplitude, η, as a Function of Frequency, f, for a Thick-Walled Inconel Tube with a Water Film Heat-Transfer Coefficient of 2675 Btu/hr·ft^2·°F.

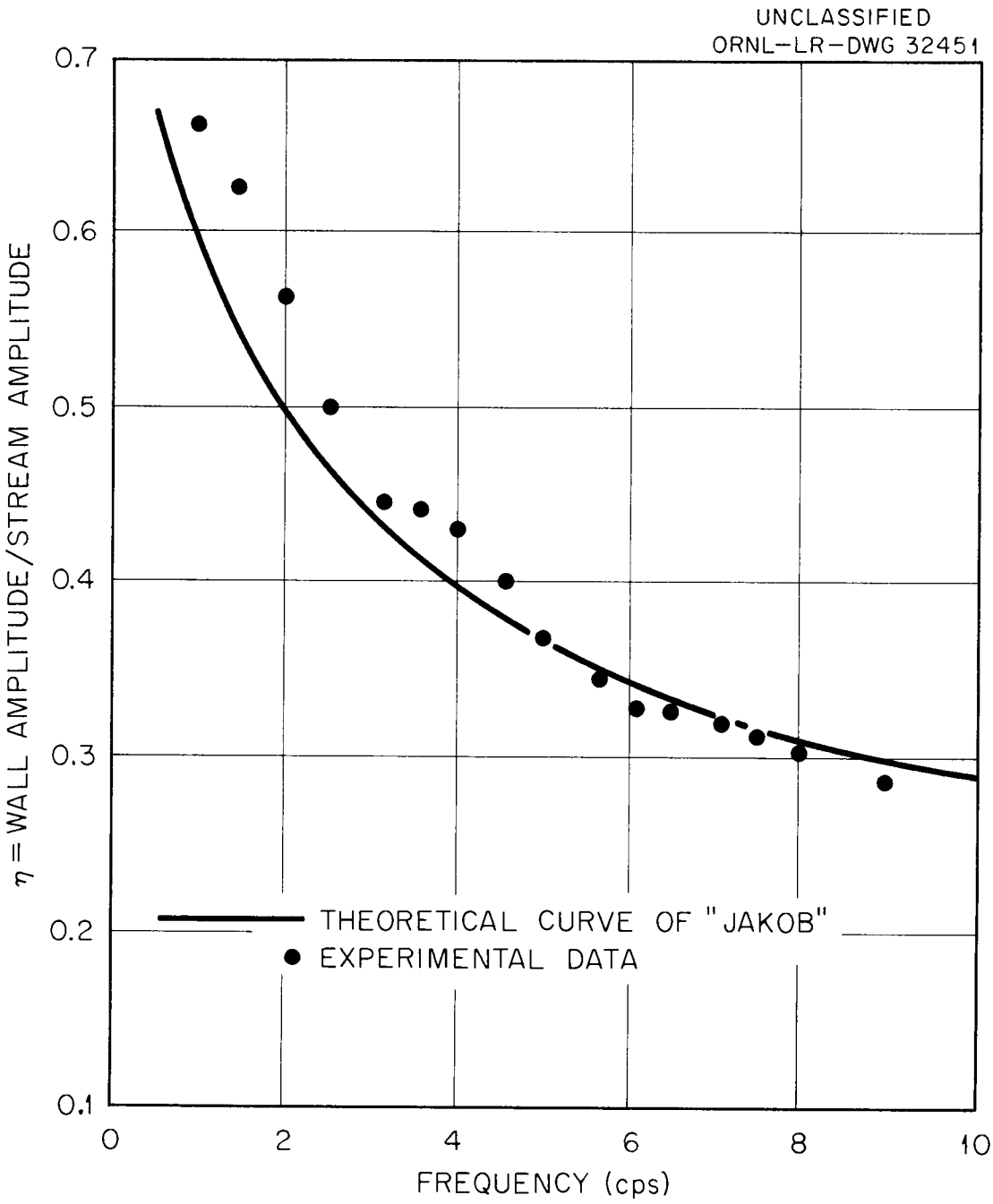

Fig. 9. Ratio of Wall Temperature Amplitude to Fluid Temperature Amplitude, η, as a Function of Frequency, f, for a Thick-Walled Inconel Tube with a Water Film Heat-Transfer Coefficient of 3700 Btu/hr·ft^2·°F.

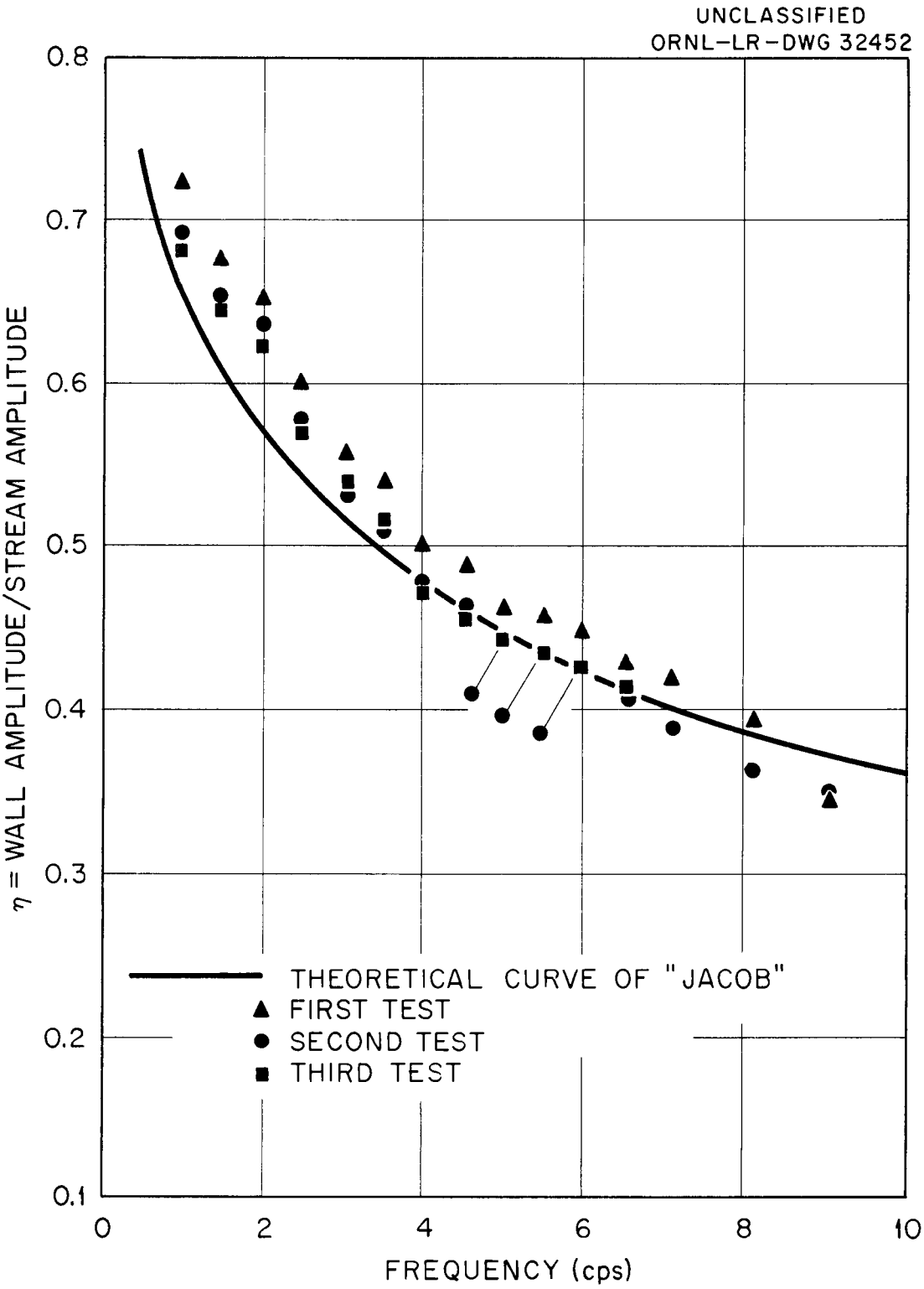

Fig. 10. Ratio of Wall Temperature Amplitude to Fluid Temperature Amplitude, η, as a Function of Frequency, f, for a Thick-Walled Inconel Tube with a Water Film Heat-Transfer Coefficient of 5000 Btu/hr·ft^2·°F

TABLE III. Properties of Inconel at 80°F[11]

$k = 8.67$ Btu/hr-ft-°F

$c = 0.109$ Btu/lb-°F

$\rho = 525.3$ lb/ft^3

$\alpha_w = 0.151$ ft^2/hr

Case II. Axial Decay in Circular Ducts

A. Negligible Heat Transfer to Wall - Velocity Profile Mixing

This case was approximated experimentally by use of a polystyrene tube, the thermal diffusivity of which is very low compared to that of metals and η approaches unity. Nevertheless, a small amount of radial heat exchange with the wall occurs, so that in comparison with theory the wall heat-transfer term (first term inside braces) in equation 21 was included. Figs. 11 and 12 depict the experimental points, along with the theoretical curves for comparisons obtained from equation 21. The dashed curves at the top of the graph are obtained from equation 20 neglecting velocity profile effects. Note that the latter predominate at all but the lower frequencies. Fig. 13 is a cross plot of Figs. 11 and 12 illustrating the flow dependence for a given tube geometry. Note that at low flows and frequencies the measured attenuation is slightly greater than predicted; whereas, at the high flows the opposite is true for low frequencies. At sufficiently high frequency, all of the measured ratios fall below theoretical, but in no case is the discrepancy more than about 12%.

A more significant comparison of theory and experiment is made by considering only that component of $A(L)/A(0)$ which is due to velocity profile mixing, as expressed in equation 18. Equation 20 is used to correct the data for the small influence of wall heat transfer, and the corrected ratio is herein designated $\left[A(L)/A(0)\right]^*$. From equation 18, it can be shown that a log-log plot of

$$\frac{-\ln\left[\frac{A(L)}{A(0)}\right]^*}{f^2} \text{ vs } N_{Re}$$

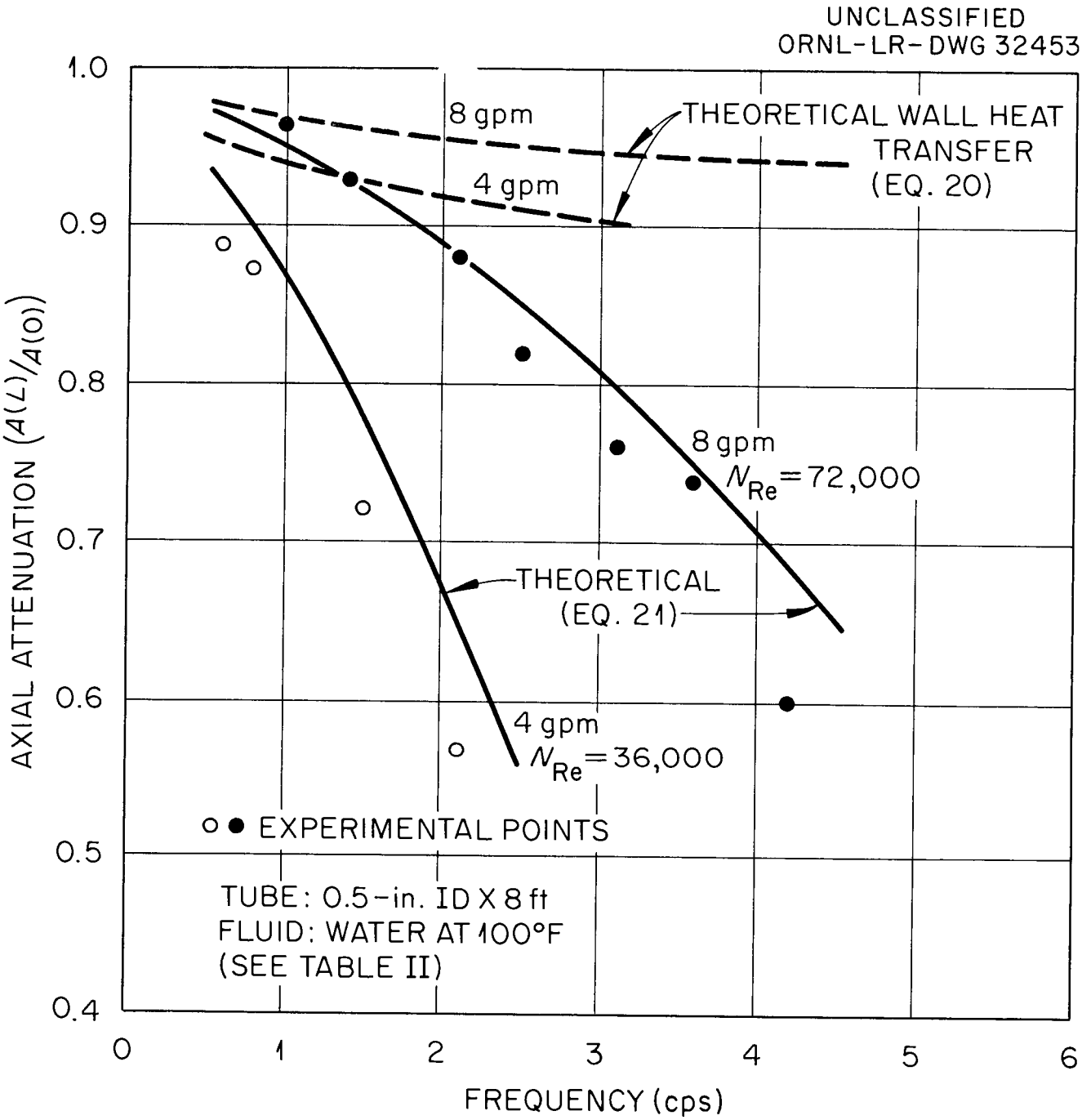

Fig. 11. Axial Attenuation in a Plastic Tube Illustrating Velocity Profile Mixing.

UNCLASSIFIED
ORNL-LR-DWG 32454

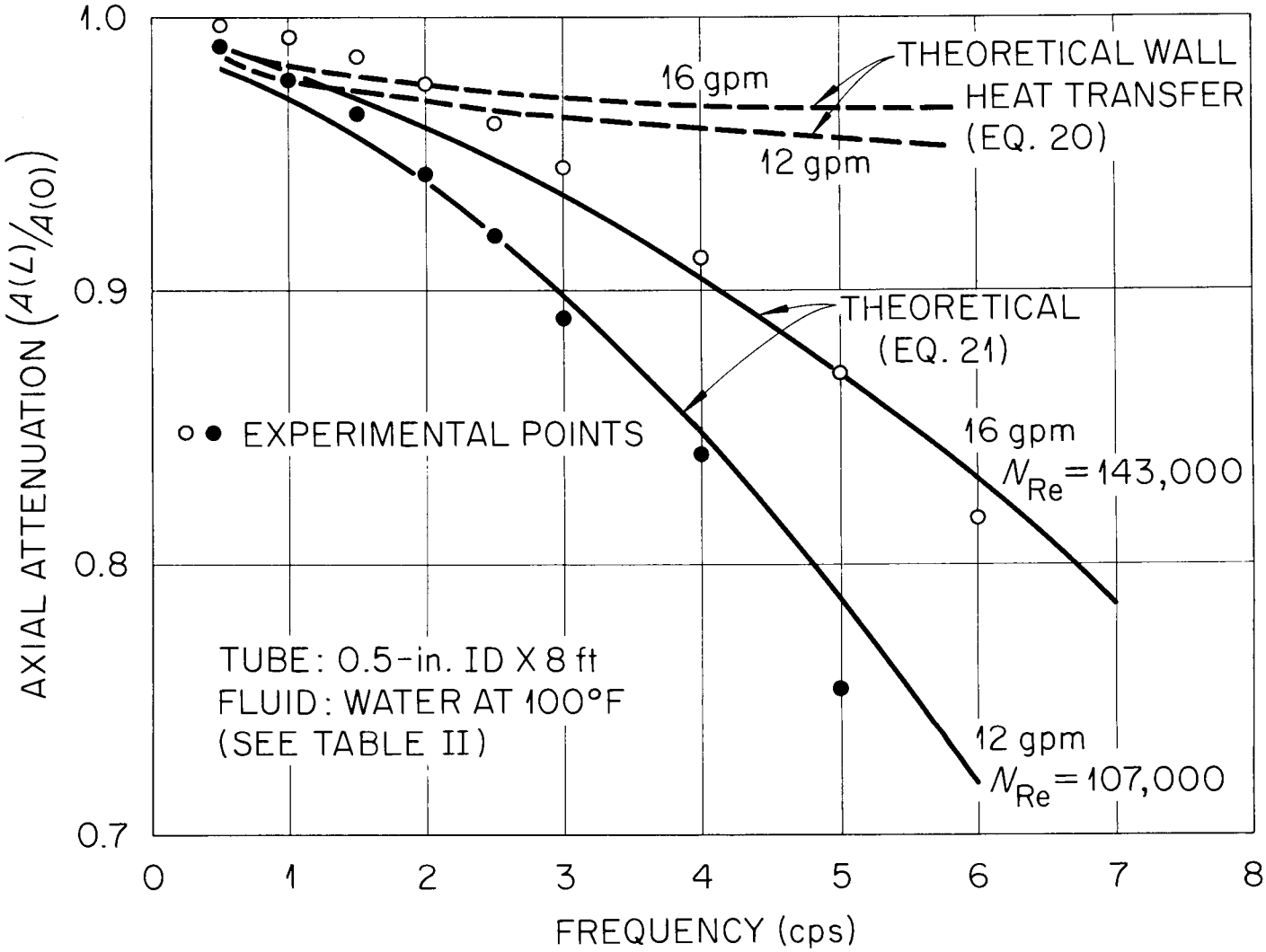

Fig. 12. Axial Attenuation in a Plastic Tube Illustrating Velocity Profile Mixing.

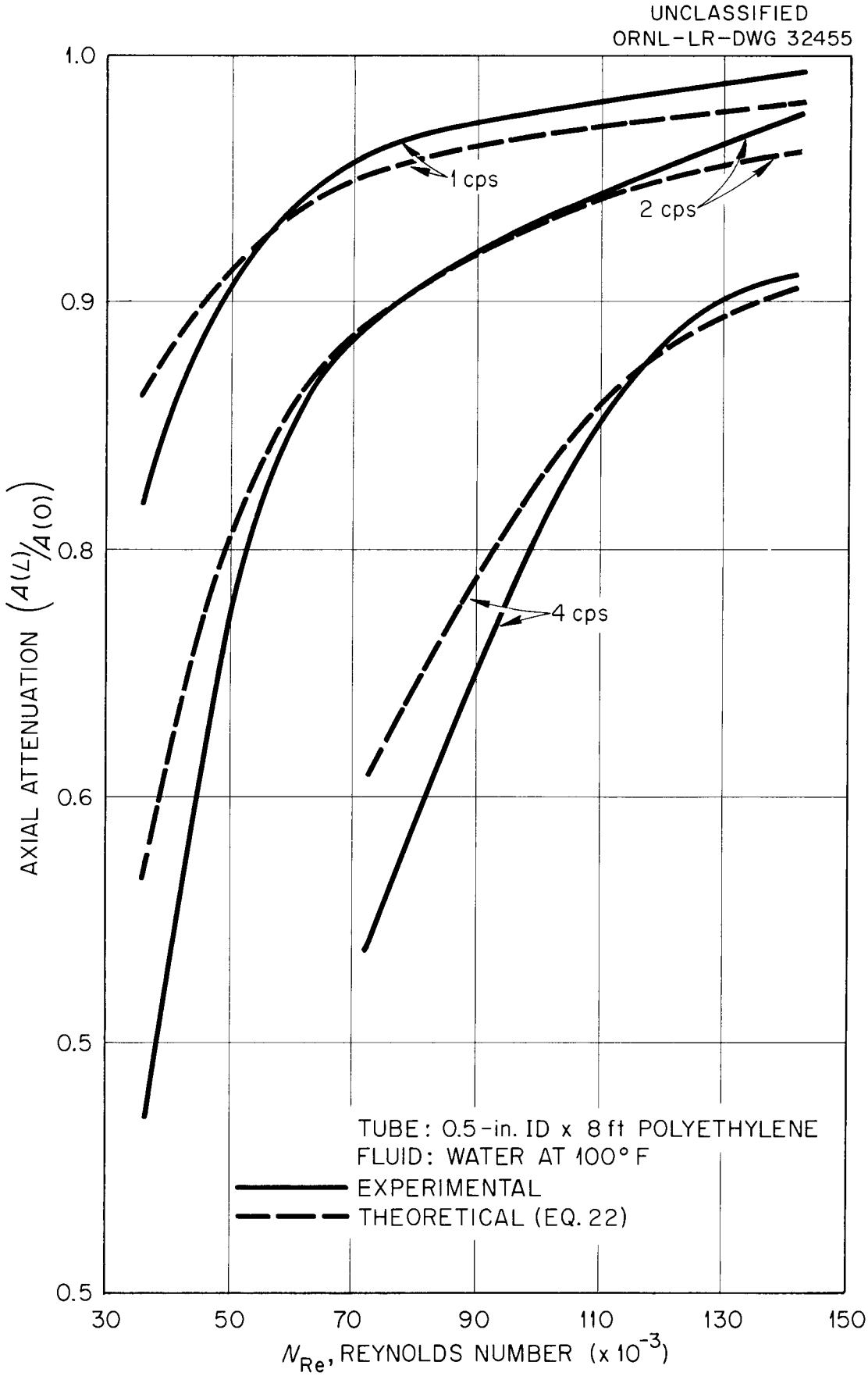

Fig. 13. Variation of Axial Attenuation with Flow Rate, Cross-Plot from Figures 11 and 12.

for a given geometry should be a straight line whose slope is -2.1, using the expression

$$f = 0.046\ N_{Re}^{-0.2}$$

in equation 18. Fig. 14 is such a plot from which two discrepancies are apparent:

1. The points taken from the corrected data do not line up linearly as predicted, especially at the higher N_{Re}. At lower N_{Re}, the experimental slopes vary from -2.8 to -3.1 as compared to -2.1 from theory of velocity profile mixing.
2. The theoretical dependence of $-\ln\left[A(L)/A(0)\right]^*$ on f^2 is not borne out by the data, with the deviations being greatest at high N_{Re}.

Discussion of possible experimental errors which may contribute to such discrepancies is deferred to a later section.

B. Axial Attenuation with Significant Heat Transfer to Wall

Two cases are to be considered: First, the pipe wall is effectively infinite, i.e., $m\ell > 2$; second, the pipe wall is thin and insulated, $m\ell < 0.5$ at 1 cps. As illustrated in Fig. 2, the principal difference in the two cases is the value of η and its frequency dependence. From equation 21, $A(L)/A(0)$ varies with η in such a way that the higher values of η correspond to lower axial attenuation, other factors remaining equal.

Data for the first case, in which the pipe wall is thick, are presented in Fig. 15 with the over-all axial attenuation, $A(L)/A(0)$, given as a function of frequency for two flow rates. Note the good agreement with

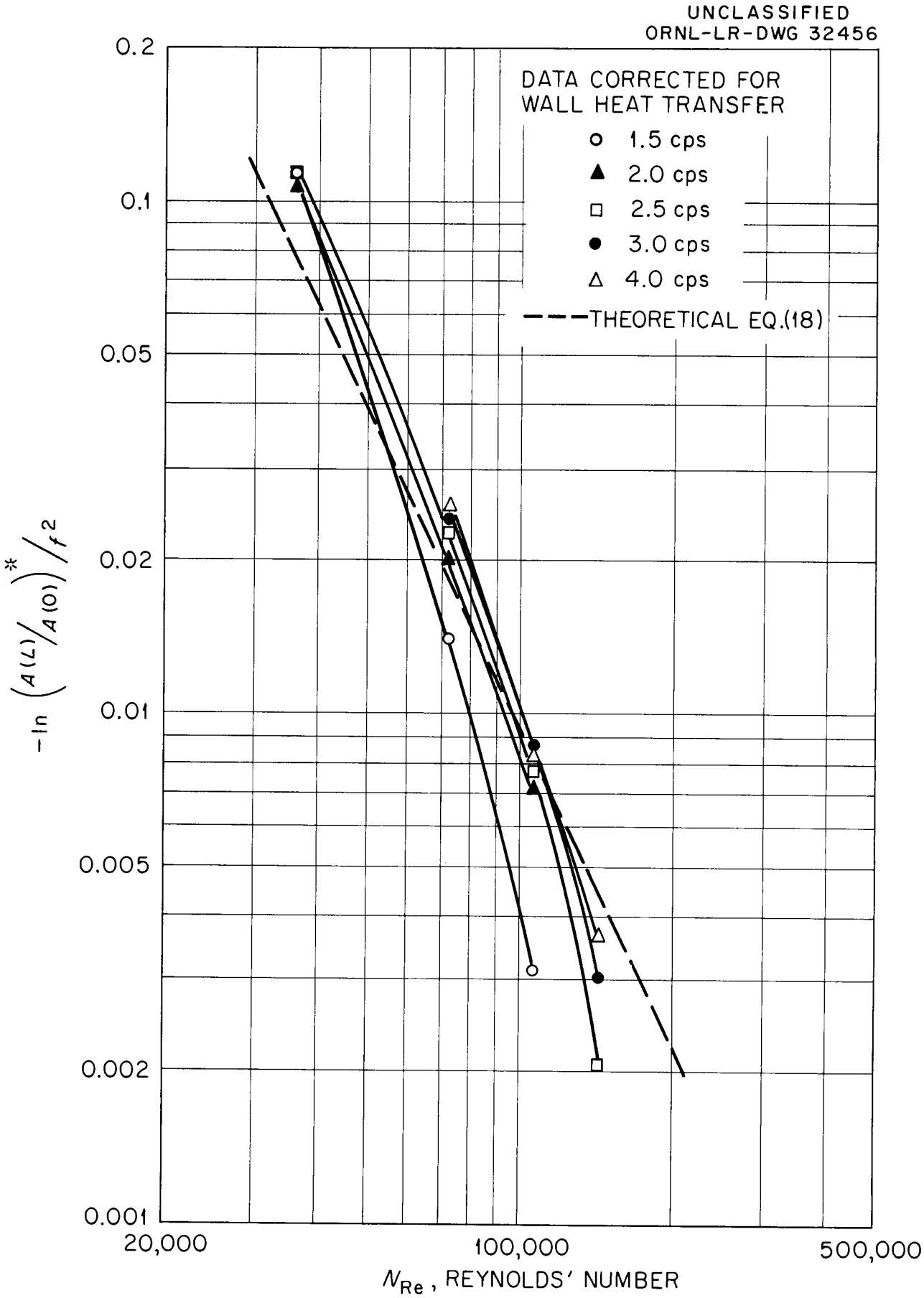

Fig. 14. Comparison of Velocity Profile Mixing With Theory: Flow and Frequency Dependence.

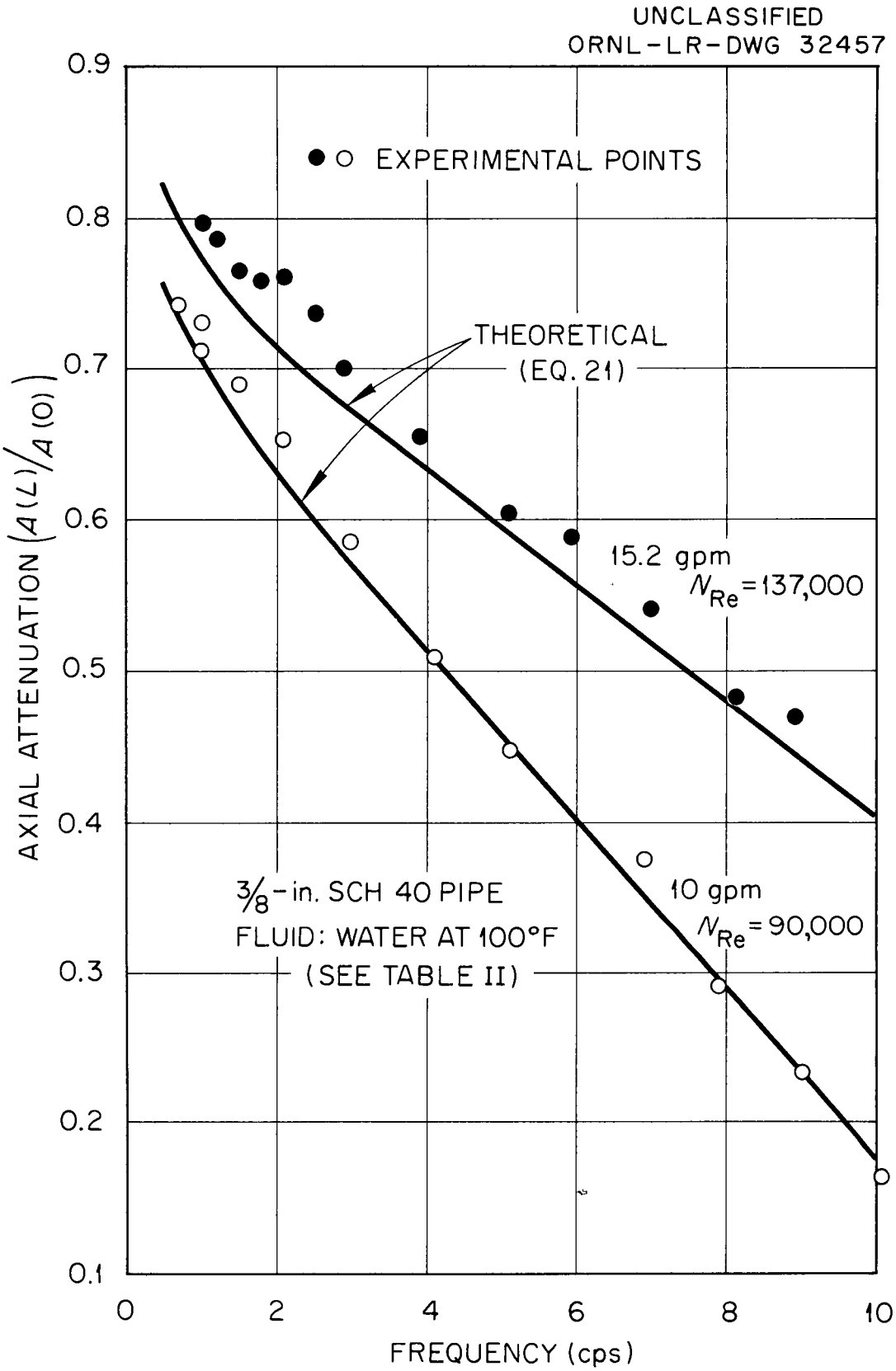

Fig. 15. Axial Attenuation in an Inconel Pipe: Comparison of Experiment with Theory.

equation 21 (solid lines) even at relatively high frequency. In the calculations, the Jakob equations (8 and 9) were used to determine η and cos ϵ.

Figs. 16 and 17 summarize the results for the second case of a thin-wall insulated tube with the solid curves computed from equation 21 using equations 13 and 14 for η and cos ϵ. In contrast with the previous case, the measured attenuation falls off more rapidly with frequency than is expected theoretically, although agreement is good for all but the lowest flow rate at frequencies below about 4 cps.

In order to elucidate the frequency and flow dependence, equation 21 can be put in a simplified form similar to equation 17:

$$\frac{A(L)}{A(0)} = \exp\left(-\frac{C\omega^j L}{G^n a}\right) \tag{22}$$

where C is a constant, j and n are exponents to be determined numerically. Over the limited frequency range from 1.5 to 8 cps, it was found that with $j = 0.575$ and $n = 0.885$ a reasonable fit to equation 22 was obtained. Fig. 18 is a graph in which the solid line is obtained from equation 22 and the points are experimental values for three frequencies. Note that significant deviation from the approximate theoretical line occurs, particularly with respect to the frequency dependence, as was observed also in Fig. 14 for the case of velocity profile mixing. The reasons for this discrepancy is not understood (see Discussion of Experimental Errors).

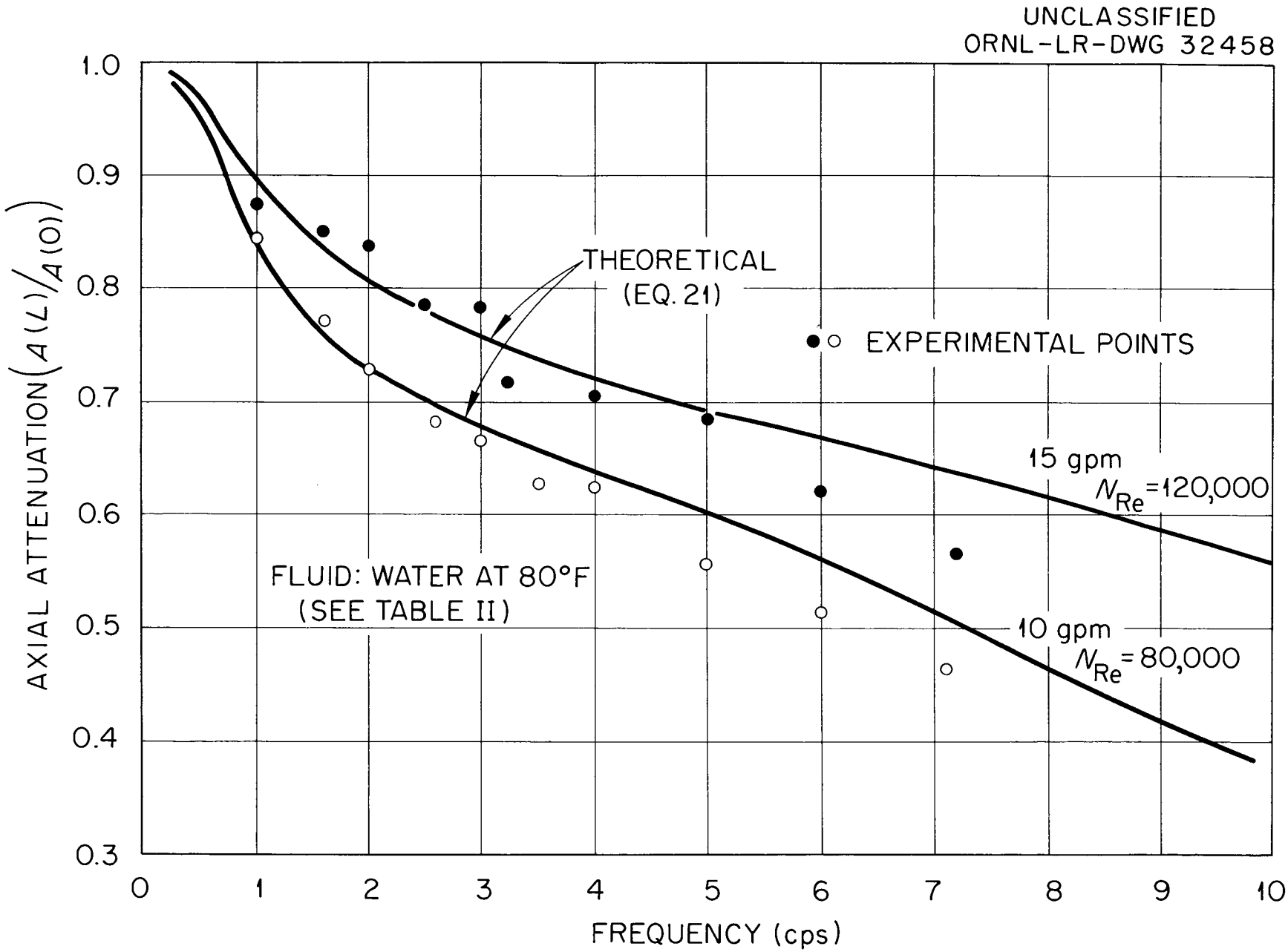

Fig. 16. Axial Attenuation in an Insulated Thin-Wall Inconel Tube: Comparison of Experiment with Theory.

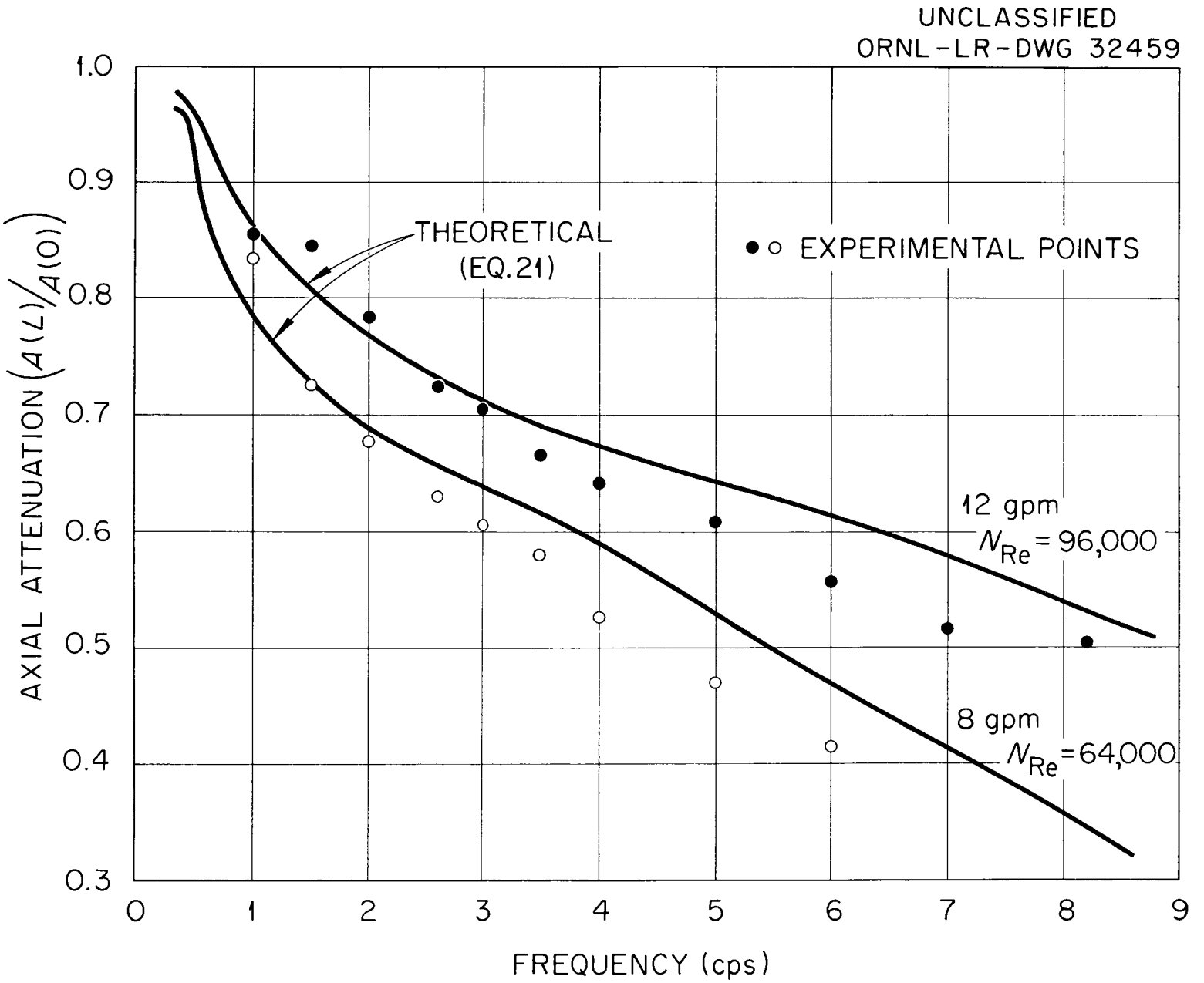

Fig. 17. Axial Attenuation in an Insulated Thin-Wall Inconel Tube: Comparison of Experiment with Theory.

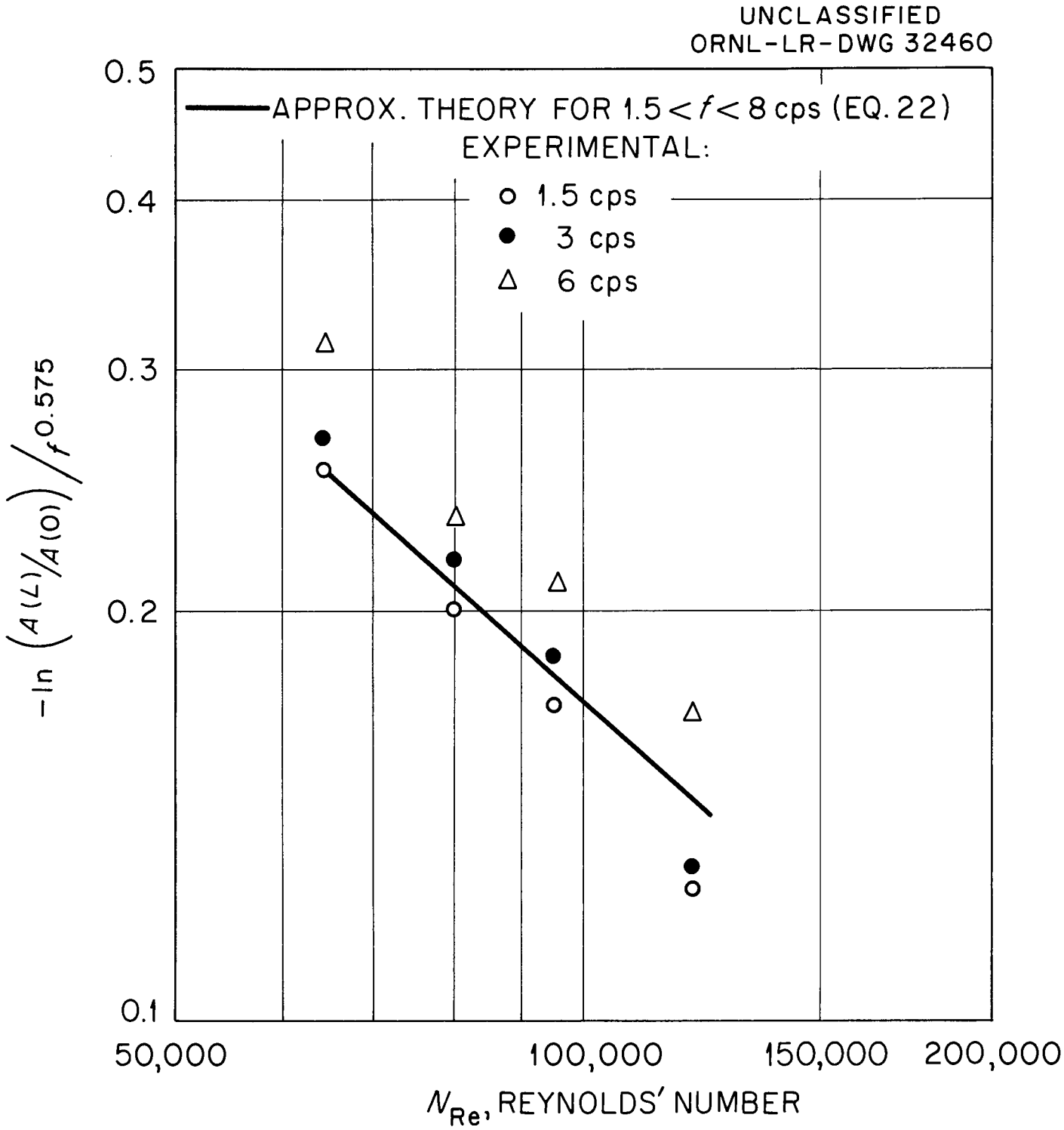

Fig. 18. Axial Attenuation in a Thin-Wall Insulated Tube: Flow and Frequency Dependence.

DISCUSSION OF EXPERIMENTAL ERRORS

It is obvious that any deviation of the experimental conditions from those assumed in the derivations can lead to discrepancies of the type found in this work. The more important sources of error in this respect include:

1. Deviation of the Wave Form from Sinusodial

This is minimized by use of the scotch-yoke drive, careful phasing of the pulse pistons, and by allowing sufficient decay ahead of the test section to damp any higher harmonics leaving the pulse generator. Nevertheless, some wave distortion occurs, especially at the higher frequencies and may account for as much as 5% error in η.

2. Variation in Fluid Properties with Temperature, especially as this causes variation in h

As discussed previously, the temperature amplitude is maintained sufficiently low so that h fluctuates no more than ± 5% about the mean value. This corresponds to considerably less than ± 5% in η, however.

3. Flow Pulsations

Small cyclic flow variations occur due to some mismatching of the pulsing pistons, variation in geometry, pressure drop, etc., between the hot and cold sides of the system. No estimate of the magnitude can be made at this time.

4. Nonadiabatic Conditions

When possible, the mean fluid temperature was adjusted to ambient to reduce heat exchange with the environment. In the case of effectively infinite wall geometry, small net heat flow is probably not serious; but for the thin-wall case where it is assumed that the outer wall is perfectly insulated, there might be a substantial effect of external heat flow. This may account for the observed greater deviations of the experiment from theory for Case II-b, thin-wall tube, as compared with Case II-A for the pipe.

5. Deviations due to Cylindrical Geometry

As discussed on page 13, it is concluded that the error should be small, probably less than 2% in η.

CONCLUSIONS

It has been demonstrated experimentally that, over a limited range at least, the approximate solutions presented in this report for local radial attenuation of temperature oscillations at an interface and for axial attenuation in circular ducts are sufficiently accurate for most engineering purposes. Closer scrutiny of the data, however, reveals some significant deviations from theory with respect to frequency and flow dependence which are not understood. It is believed that a more refined theoretical approach taking into account the thermal capacity of the boundary layer (see note, page 9), as well as a more precise definition of the effective axial diffusivity in terms of heat transfer, should be attempted in order to ascertain whether the observed discrepancies are due to the theoretical assumptions or are the result of direct experimental error.

The "gunbarrel" thermocouple technique appears to be an excellent one for measurement of instantaneous surface temperatures in thick metallic walls.

Extension of this investigation to the thermal entrance region in circular ducts is anticipated.

ACKNOWLEDGEMENT

The authors wish to acknowledge the assistance of F. J. Schafer in carrying out the experiments and in data analysis.

REFERENCES

1. Hanratty, T. J., "Turbulent Exchange of Mass and Momentum with a Boundary," AIChE Journal, 2, 359 (1956).

2. Mott, J. E., "An Investigation of Thermal Transients at a Solid-Fluid Interface," ORNL-CF 57-10-122.

3. Jakob, M., Heat Transfer, Vol. I, John Wiley and Sons, New York, p 298 (1949).

4. Platus, D. H., and Meghreblian, R. V., "Conduction of Heat in a Finite Plate in Contact with an Environment in which the Temperature Varies as a Prescribed Function of Time," ORNL-CF 56-9-60.

5. Platus, D. H., "Conduction of Heat in a Finite Plate in Contact with an Environment in which the Temperature Varies as a Prescribed Function of Time," ORNL-CF 56-9-60, Addendum 1.

6. Taylor, G. I., "The Dispersion of Matter in Turbulent Flow Through a Pipe," Proc. Roy. Soc. (London) A 223, 446, May, 1954.

7. Tichacek, L. S., and Barkelew, Baron T., "Axial Mixing in Pipes," AIChE Journal, 3, 439 (1957).

8. Keyes, J. J., "Diffusional Film Characteristics in Turbulent Flow: Dynamic Response Method," AIChE Journal, 1, 305 (1955).

9. Thompson, J. J., "The Effect of Turbulent Diffusion on Temperature Transients in Liquid Metal Fuel Reactor Pipelines," AERE-R/R-2365 (Harwell), (1957).

10. McAdams, W. H., Heat Transmission, 2nd Ed., 168, McGraw-Hill Book Company, New York (1942).

11. Lyman, T., (Ed.), Metals Handbook, American Society for Metals, p 1057 (1948).

12. Karman, T. von, Mathematical Methods in Engineering, McGraw-Hill Book Company, New York (1940).

APPENDIX I

DEVIATION OF CASE I-B: Local Attenuation at an Interface-Finite Plate, Adiabatic

The basic differential equation is equation 3 (page 7)

$$\frac{\partial^2\theta(x',\tau)}{\partial x'^2} = -\frac{1}{\alpha_w}\frac{\partial\theta(x',\tau)}{\partial\tau} \tag{24}$$

with boundary conditions as given by equations 5 and 11. Note that x' $(= \ell - x)$ is the distance measured from the insulated face:

$$h\left[\theta_e(\tau) - \theta(\ell,\tau)\right] = k_w \frac{\partial\,(x',\tau)}{\partial x'} \qquad \text{at } x' = \ell \tag{25}$$

where $\theta_e(\tau) = A_e \cos \omega\tau$;

$$\frac{\partial\theta(x',\tau)}{\partial x'} = 0 \qquad \text{at } x' = 0 \tag{26}$$

Following the procedure of von Karman and Biot[12] as illustrated in Appendix II, it is permissible to set

$$\vec{\theta}(x,\tau) = A(x) \exp(i\omega\tau) \quad ,^{*} \tag{27}$$

analogous to equation 41, as a solution to equation 24.

Substituting equation 27 back into equation 24:

$$\frac{d^2\,\vec{A}(x)}{dx^2} = \frac{i\omega\,\vec{A}(x)}{\alpha_w} \tag{28}$$

Likewise, the two boundary conditions transform:

$$h\left[\vec{A}_e - \vec{A}(\ell)\right] = k_w \frac{d\,\vec{A}(x')}{dx'} \qquad \text{at } x' = \ell \tag{29}$$

---

*Note that the arrow over a symbol is used to denote a complex quantity.

$$\frac{d\,\vec{A}(x')}{dx'} = 0 \qquad \text{at } x' = 0 \tag{30}$$

Solving equation 28, with equation 30:

$$\vec{A}(x') = c' \cosh\,(1 - i)\,mx'$$

$$\therefore \quad k\,\frac{d\,\vec{A}(x')}{dx'} = cmk_w\,(1 - i)\,\sinh\,(1 - i)\,mx' = h\left[\vec{A}_e - \vec{A}(\ell)\right] \tag{31}$$

But

$$\vec{A}(\ell) = c\,\cosh\,(1 - i)\,m\ell \quad , \tag{32}$$

and

$$\frac{\vec{A}_e - \vec{A}(\ell)}{\vec{A}_e} = 1 - \vec{\eta} \tag{33}$$

Combining equation 32 and 33 with 31:

$$\vec{\eta} = \left[\frac{mk_w}{h}\,(1 - i)\,\tanh\,(1 - i)\,m\ell + 1\right]^{-1} \tag{34}$$

$$= A + iB$$

Comparing terms,

$$A = \frac{\delta\xi}{\delta^2 + (m\beta/b)^2} \tag{35}$$

$$B = \frac{(m/b)\,\beta\xi}{\delta^2 + (m\beta/b)^2} \tag{36}$$

$$\beta = \sinh 2\,m\ell + \sin 2\,m\ell$$

$$\delta = m/b\,(\sinh 2\,m\ell - \sin 2\,m\ell) + \cosh 2\,m\ell + \cos 2\,m\ell$$

$$\xi = \cosh 2\,m\ell + \cos 2\,m\ell$$

$$\eta = \left|\vec{\eta}\right| = (A^2 + B^2)^{1/2}$$
$$= \frac{\zeta}{\left[\delta^2 + (m\beta/b)^2\right]^{1/2}} \tag{37}$$

which is equation 13 of the text.

Note that by letting $\ell \to \infty$ in the above equation, the Jakob equation (page 9) is obtained.

APPENDIX II

DERIVATION OF CASE II, B-1: Axial Attenuation of Sinusoidal Fluid Temperature Oscillations in Circular Ducts - Velocity Profile Mixing Neglected

Consider plug flow in an insulated pipe of radius a with inlet fluid temperature given by

$$\theta(0,\tau) = A(0) \cos \omega\tau \tag{38}$$

From differential heat and material balances across a volume element, dz:

$$\frac{2q}{a} + cG \frac{\partial\theta(z,\tau)}{\partial z} + c\rho \frac{\partial\theta(z,\tau)}{\partial\tau} = 0 \tag{39}$$

where q is the instantaneous wall heat flux. Note that longitudinal conduction has been neglected in equation 39. Fluid properties are assumed independent of temperature.

The method of solution is that described by von Karman and Biot[12] for the steady state. The desired solution, subject to the harmonic boundary condition at z = 0 (equation 38), is of the form:

$$\theta(z,\tau) = A(0) \exp\left[-R(z)\right] \cos\left[\omega\tau - \Phi(z)\right] \tag{40}$$

Since any linear combination of $\cos\left[\omega\tau - \Phi(z)\right]$ and $\sin\left[\omega\tau - \Phi(z)\right]$ is a solution of equation 39, in particular

$$\vec{\theta}(z,\tau) = A(0) \exp\left[-R(z)\right]\left\{ \cos\left[\omega\tau - \Phi(z)\right] + i \sin\left[\omega\tau - \Phi(z)\right] \right\}$$

is also a solution.

$$\therefore \quad \vec{\theta}(z,\tau) = A(0) \exp\left[-R(z)\right] \exp i\left[\omega\tau - \Phi(z)\right] \quad .$$

$$\vec{\theta}(z,\tau) = \vec{A}(z) \exp(i\omega\tau) \quad , \tag{41}$$

where

$$\vec{A}(z) = A(0) \exp\left[-R(z) - i\Phi(z)\right] \quad . \tag{42}$$

$\vec{A}(z)$ is the complex thermal amplitude at z. Thus if a solution for $\vec{A}(z)$ can be found, the real part of the solution gives for the amplitude

$$A(z) = A(0) \exp\left[-R(z)\right] \quad ; \tag{43}$$

the phase shift, $\Phi(z)$, can be found from the imaginary part of the solution.

The attenuation ratio for length L is, accordingly,

$$\frac{A(L)}{A(0)} = \exp\left[-R(L)\right] \tag{44}$$

and the phase shift is $\Phi(L)$.

Substituting equation 41 into the differential equation 39

$$\frac{2\vec{q}}{a} + cG\,\frac{d\vec{A}(z)}{dz} + i\,c\rho\omega\,\vec{A}(z) = 0 \tag{45}$$

Note that the above substitution transforms the partial into an ordinary differential equation in the variable z.

Auxiliary Condition

Let the complex radial attenuation ratio, $\vec{\eta}$, be defined:

$$\vec{\eta} = \frac{\vec{A}_i(z)}{\vec{A}(z)} \quad , \tag{46}$$

being independent of position, z, along the tube.

The instantaneous heat flux, q, in equation 39, can be related to the local film coefficient, h, and temperature drop, employing assumption (2) (page 8) which is equivalent to neglecting thermal capacity of the boundary layer.

Thus,

$$q = h\left[\theta(z,\tau) - \theta_i(z,\tau)\right] \tag{47}$$

Substitution of equation 41 in equation 47:

$$\vec{q} = h\left[\vec{A}(z) - \vec{A}_i(z)\right] + iI \tag{48}$$

From equations 46 and 48

$$\vec{q} = h(1 - \vec{\eta})\,\vec{A}(z) + iI \quad , \tag{49}$$

where I designates the imaginary part of the solution, not of interest here.

The differential equation to be solved is obtained by combining equations 45 and 49:

$$\frac{2h(1 - \vec{\eta})\,\vec{A}(z)}{a} + cG\,\frac{d\vec{A}(z)}{dz} + i\,c\rho\omega\,\vec{A}(z) = 0 \tag{50}$$

Taking

$$\vec{\eta} = A + iB \quad , \tag{51}$$

and letting

$$\vec{A}(z) = A(0) \qquad \text{at } z = 0 \quad ,$$

the solution of equation 50 is:

$$\frac{\vec{A}(z)}{A(0)} = \exp\left[-\frac{2h}{acG}(1 - A) + i\left(\frac{\rho\omega}{G} + I'\right)\right]z \tag{52}$$

Comparing equation 52 with equation 43,

$$R(z) = \frac{2hz}{acG}(1 - A) \tag{53}$$

$\Phi(z) = -\left(\frac{\rho\omega}{G} + I'\right)$ is not of particular interest here.

In order to complete the solution, an additional approximation is made:

$$\eta = \left| \vec{\eta} \right| = \sqrt{A^2 + B^2}$$

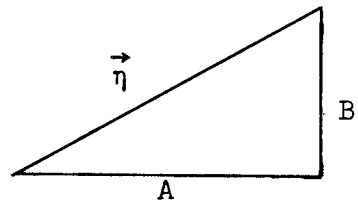

It can be shown that, for $\epsilon = \tan^{-1} B/A < 35$ deg, a good approximation is had by setting

$$A \cong \eta \cos \epsilon \tag{54}$$

where η is the appropriate surface attenuation ratio, and ϵ is the corresponding phase shift. See Fig. 3 for a graph of $\eta \cos \epsilon$ vs η.

From equations 44, 53, and 54, at $z = L$:

$$\frac{A(L)}{A(0)} \cong \exp\left[- \frac{2hL}{acG} (1 - \eta \cos \epsilon) \right] \tag{55}$$

which is equation 20 of the text with $G = \rho U$.

INTERNAL DISTRIBUTION

1. D. S. Billington
2. F. F. Blankenship
3. E. P. Blizard
4. A. L. Boch
5. C. J. Borkowski
6. G. E. Boyd
7. E. J. Breeding
8. R. B. Briggs
9. C. E. Center (K-25)
10. R. A. Charpie
11. F. L. Culler
12. D. A. Douglas, Jr.
13. L. B. Emlet (K-25)
14. D. E. Ferguson
15. J. Foster
16. A. P. Fraas
17. J. H. Frye, Jr.
18. W. R. Gambill
19. B. L. Greenstreet
20. W. R. Grimes
21. A. G. Grindell
22. E. Guth
23. C. S. Harrill
24. H. W. Hoffman
25. A. Hollaender
26. A. S. Householder
27. W. H. Jordan
28. P. R. Kasten
29. G. W. Keilholtz
30. M. T. Kelley
31-32. J. J. Keyes, Jr.
33. R. B. Korsmeyer
34. A. I. Krakoviak
35. C. G. Lawson
36. J. A. Lane
37. R. S. Livingston
38. F. E. Lynch
39. H. G. MacPherson
40. W. D. Manly
41. J. R. McNally
42. H. J. Metz
43. K. Z. Morgan
44-45. J. E. Mott
46. J. P. Murray (Y-12)
47. R. H. Nimmo
48. M. L. Nelson
49. A. M. Perry
50. C. A. Preskitt
51. G. Samuels
52. H. W. Savage
53. A. W. Savolainen
54. F. J. Schafer
55. H. E. Seagren
56. E. D. Shipley
57. M. J. Skinner
58. A. H. Snell
59. I. Spiewak
60. W. J. Stelzman
61. J. A. Swartout
62. E. H. Taylor
63. D. B. Trauger
64. J. L. Wantland
65. A. M. Weinberg
66. C. E. Winters
67. Health Physics Library
68. Biology Library
69. Reactor Experimental Engineering Library
70-71. Central Research Library
72-91. Laboratory Records Department
92. Laboratory Records, ORNL R.C.
93. ORNL - Y-12 Technical Library, Document Reference Section

EXTERNAL DISTRIBUTION

94. Division of Research and Development, AEC, ORO
95-627. Given distribution as shown in TID-4500 (14th ed.) under Physics and Mathematics category